Received: 17 August 2021 | Revised: 1 May 2022 | Accepted: 23 May 2022

DOI: 10.33012/navi.543

ORIGINAL ARTICLE

Signal Quality Monitoring Based on Chip Domain Observables: Theory, Design, and Implementation

Xiang Wang[1] | **Xiaowei Cui**[1] | **Gang Liu**[1] | **Kefan Wei**[2] | **Mingquan Lu**[1,3]

[1] Department of Electronic Engineering, Tsinghua University, Beijing 100084, China

[2] North Information Control Research Academy Group Co. Ltd., Nanjing 211153, China

[3] Beijing National Research Center for Information Science and Technology, Tsinghua University, Beijing 100084, China

Correspondence
Xiaowei Cui, Department of Electronic Engineering, Tsinghua University, Beijing 100084, China.
Email: cxw2005@tsinghua.edu.cn

Abstract

Signal quality monitoring (SQM) is a technique utilized by satellite- and ground-based augmentation systems (SBAS/GBAS) to detect potential hazardous deformations in signals and better protect integrity for safety-critical users. The next generation of SBASs will incorporate dual-frequency multi-constellation (DFMC) techniques, for which SQM is particularly important since signal deformations might be the largest source of uncertainty in ranging error after first-order ionospheric delays are eliminated. However, the performance bounds of the traditional multi-correlator-based SQM technique face some challenges because of the raised requirement on detection sensitivity by dual-frequency ionosphere-free measurements and multiple modulation modes of civilian signals from multi-constellation techniques. To mitigate the challenges and improve overall performance, SQM based on chip domain observables (CDOs) is emerging, but has not yet been systematically studied. We propose a design methodology for CDO-based SQM, consisting of derivations and corresponding massive simulations. Correctness and effectiveness are assessed to confirm the methodology, and a simplification process by checking the sensitivity of CDOs is demonstrated in terms of implementation.

Keywords

chip domain observable, CDO, design methodology, dual-frequency multi-constellation, DFMC, satellite-based augmentation system, SBAS, signal quality monitoring, SQM

1 | INTRODUCTION

Thanks to the ongoing modernization of GPS and GLONASS, as well as the rapid development of Galileo and the BeiDou navigation satellite systems (BDS), the four global navigation satellite systems (GNSSs) provide positioning, navigation, and timing services for users in a growing number of application fields. However, for some safety-critical application scenarios (e.g., precision approaches in civil aviation), there exist some extra requirements beyond the basic performance of GNSS core constellations. Therefore, some satellite- and ground-based augmentation systems (SBAS/GBAS) have been developed as important supplements to GNSSs in

that they provide corrections to improve accuracy and address threats to enhance integrity.

The next generation of SBASs will incorporate dual-frequency multi-constellation (DFMC) techniques, which would eliminate first-order ionospheric error and provide observation redundancy to better mitigate potential integrity risks and promote availability for safety-critical application scenarios (Walter, 2012). However, the relative magnitudes of other sources of ranging errors might become more significant. One of these significant error sources is signal deformation, which might act as the largest source of ranging uncertainty (Walter, 2012). There are many potential causes of deformations in received signals, such as the radio-frequency (RF) front-end processing of a ground receiver, the multipath effect of site environment, malfunctions or imperfections of signal generating hardware onboard satellites, and so on.

In this article, the term *signal deformation* refers specifically to an evil waveform (EWF) that is caused by the above onboard hardware failures (i.e., the signal-in-space [SIS] has already been deformed since emission). Signal tracking is sensitive to configurations of a ground receiver, including the discriminator type of the tracking loop, the correlator spacing, and properties of the pre-correlation filter such as a 3-dB bandwidth, differential group delay, and roll-off rate out of band. As a consequence, reference and user receivers with different configurations might track EWFs differently, invalidating the differential process or further introducing large differential pseudorange errors to various users. To mitigate EWF risks, a technique called signal quality monitoring (SQM) was developed that measures a set of metric values with the monitored incoming signal to find if any corresponding thresholds have been exceeded, thus identifying whether there was the presence of an EWF.

Note that an EWF might mislead different receivers with different configurations differently (Phelts, 2001). Given a prescribed receiver configuration space, the task of SQM is to ensure that all the possible EWFs that could cause maximum differential pseudorange errors to exceed a predefined limit can be detected. Therefore, intuitive SQM might be carried out by monitoring pseudorange differences among various receiver configurations with the same signal. However, there is usually one code tracking loop within a receiving channel, thereby inducing the need to deploy a large number of receivers to cover the specified user receiver configuration space (URCS). Thus, pseudorange-based SQM is complicated, budget-consuming, and impractical (Phelts, 2001). Subsequently, the receiver channel with multiple pairs of early-minus-late (E-L) correlators was developed to detect potential deformations in correlation peaks.

Operational metrics of the SQM methods based on multi-correlator observables (MCOs) include overall metrics reflecting the whole shape of the correlation peak utilizing all the correlator values, e.g., α-metric once applied by the monitors on the Wide Area Augmentation System (WAAS; Phelts, 2003), and local metrics representing the slopes and/or symmetries of different parts on the correlation peak by applying particular correlator values, e.g., Δ-test and ratio-test used by SQM2b (Phelts, 2001) monitors the current European Geostationary Navigation Overlay Service (EGNOS; Pagot, 2018; Selmi, 2020).

The MCO-based SQMs have been operational for nearly two decades and perform well in single-frequency SBASs. However, the filtering effect of the correlating process might average down some distortions, indicating a limited detection performance of MCO-based SQM. Furthermore, new requirements are raised by DFMC SBASs that are in the process of standardization. On the one hand, traditional performance bounds are facing challenges from higher demands on detection sensitivity that are raised by the error-inflating effect of dual-frequency (DF) iono-free measurements (Phelts, 2013). On the other hand, in expanding from the

traditional binary phase shift keying (BPSK) modulated signals to the emerging binary offset carrier (BOC) modulated ones, the applicability of MCO-based SQM is affected by the different magnitudes of potential deformations due to different chip rates and different slopes of correlation peaks. To mitigate these challenges, a signal-level SQM method based on chip domain observables (CDOs) was developed, since the chips of various modulations act quite similarly in transitions, which benefits the CDO-based SQM by being less modulation-dependent.

The concept of CDOs was first introduced by NovAtel Inc. during the development of the Vision Correlator, where an extensive application of SQM was also mentioned (Fenton, 2005). Later, a signal compression algorithm was proposed by Weill (2007), which explained the mechanism of the Vision Correlator and generalized it to an approach for any GNSS signals to be compressed to obtain precise determinations of high-resolution chip waveforms and cross-correlation functions. Before Vision-Correlator-equipped NovAtel G-III receivers were deployed at WAAS reference stations, Phelts (2013) proved that CDO-based metrics were sensitive enough and far better than MCO-based metrics for SQM and could be easily applied to L1 and L5 signals. Nevertheless, a concrete algorithm or a detailed design methodology was not released.

Based on high-gain parabolic dish antennas, Thevenon (2014), Pagot (2015), and Li (2017) promoted research on signal visualization, including computations of CDOs, assessment of signal quality consistencies, etc. He (2018) also proposed a waveform rising and falling edge symmetry (WRaFES) model with 24 metrics for measuring symmetries between rising and falling edges. However, signal visualization approaches under high carrier-to-noise ratios (C/N_0) and/or very high sampling frequency conditions are not suitable for operational SQM on SBAS reference stations. On the contrary, Wang (2021a) demonstrated a specific CDO-based SQM algorithm in the conditions of omnidirectional antennas and summarized the advantages with the BDS B1C signal compared to the traditional method. Notwithstanding, the potential of CDO-based SQM was not fully explored, evaluated, or exploited.

From pseudorange-based to multi-correlator-based to chip-waveform-based SQMs, detection metrics have been defined on observables from pseudorange differences to correlation shapes, then to chip shapes correspondingly, in order to mitigate reductions of original information. Detection sensitivity has, hence, progressively enhanced. Theoretically, the noise level of CDO-based metrics is higher than that of traditional MCO-based metrics. Nevertheless, Thevenon (2014) highlighted the properties of high temporal resolution and additive Gaussian white noise (AWGN) of RF front-end outputs, which enable CDO-based metrics the advantage of processing particular segments of chip waveforms to estimate certain parameters. Provided with the operational procedure of SQM and DFMC SBAS requirements, this article proposes a detailed and concrete methodology to design CDO-based SQM for a DFMC SBAS. Additionally, an algorithmic scheme based on multiple representative civilian signals with different modulations is developed by applying the proposed methodology.

This article is organized as follows. Section 2 introduces the fundamentals of SQM and some external conditions common for SQM methods, including threat modeling issues and receiver configuration constraints. Based on the operational procedure described in Section 3, a methodology for the design and implementation of CDO-based SQM is proposed, for which a verification platform is designed as well. Section 4 develops a CDO-based SQM design approach based on derivations and the corresponding massive simulations on influential factors resulting in a generic baseline algorithm. Section 5 provides assessments in some cases, followed by a demonstration of the simplification process of the designed baseline

algorithm by examining the sensitivities of metrics. Section 6 concludes the work and envisions some directions for future study.

2 | CONTEXTS OF THIS STUDY

A typical SBAS (e.g., the legacy and/or the modernized WAAS [Walter, 2012]) conventionally consists of several integrity monitors, where only SQM provides a connection between the signal domain where detections are actually carried out and the ranging domain where pseudoranges are measured. Development of SQM was stimulated by the need to monitor potential distortions in GNSS signals. To clarify the concepts of SQM, several aspects of context are introduced in this section.

2.1 | Fundamentals of SQM

Note that a signal deformation refers specifically to an EWF caused by satellite problems in this article. Since the first observed occurrence (i.e., the SVN-19 Event in 1993), several deformation events have been observed on GPS civil signals. Shallberg (2017) summarized these deformations into four types:

- deformed signals caused by failures of signal generating hardware onboard GPS satellites
- signals with slight distortions from satellite operations
- signals with satellite-induced elevation-dependent code biases (e.g., GPS SVN-49 signals)
- deformed signals relevant to WAAS geostationary Earth orbit (GEO) satellite failures

No matter how clear the mechanisms are, the latter three types of signal deformations could be deemed as scheduled or specific under certain conditions and are, therefore, preventable and/or controllable, relatively. Signal deformations of the first type, on the other hand, are unscheduled and random, with the potential to cause hazardous misleading information (HMI) to be sent to users and, thus, must be addressed. As a consequence, an EWF further refers to a deformed signal emitted by a satellite with malfunctions and/or imperfections in signal generation hardware onboard.

An SBAS is essentially a wide-area differential system, improving positioning accuracies by broadcasting differential corrections from GEOs. If an EWF were received, the cross-correlation function of the distorted incoming signal and nominal local replica would be deformed (Phelts, 2001; i.e., fail to sustain the nominal slope and/or symmetry of the correlation peak). Since signal tracking is sensitive to receiver configurations, an EWF could invalidate or even worsen the differential process. Consequently, the SQM technique was developed to mitigate the potential for HMI induced by EWFs. Figure 1 shows an example of a simulated GPS L1 C/A signal with distortions, where all three receivers have the same pre-correlation bandwidths (PCBw) but different correlator spacings. Taking Figure 1(a) with 0.10-chip spacing as the reference, the User I receiver in Figure 1(b) with 0.20-chip spacing would suffer an error of 0.0225 chips, equivalent to 6.594 meters. Those of User II in Figure 1(c) would be an error of 0.0117 chips or 3.429 meters, respectively.

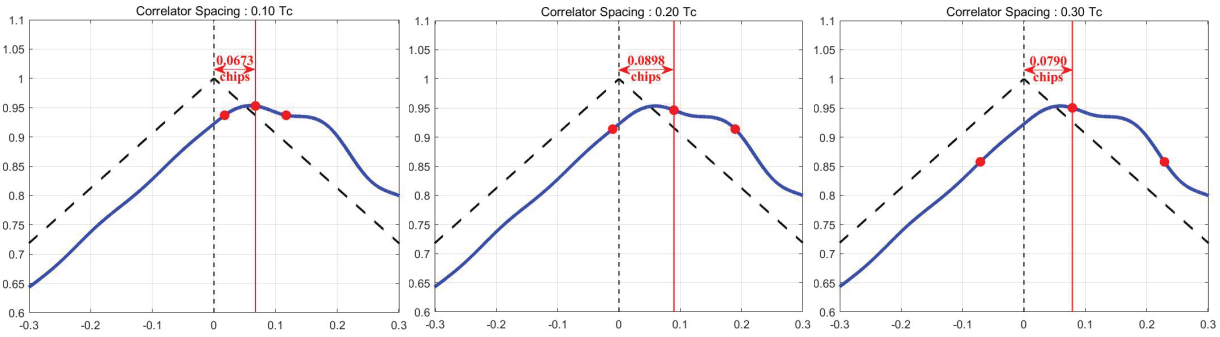

(a) Reference (b) User-I (c) User-II

FIGURE 1 Different tracking errors suffered by tracking pairs with different spacings

2.2 | External Conditions for the Design of an SQM Method

The performance of an SQM method lies in its ability to protect safety-critical users against unreasonably large differential ranging errors and alert users in time based on detection. The generality, reliability, and availability of an SQM method are determined by three aspects of external conditions:

- representative signals with various modulations
- threatening anomalous data set for tests
- receiver configuration space to be protected

2.2.1 | Considered Modulations of Signals to Protect

An SBAS is an example of a civilian-oriented system for integrity augmentation. Civil GNSS signals are conventionally transmitted on L1/E1/B1 and L5/E5/B2 frequencies, with modulation modes of BPSK(1), BOC(1,1), and BPSK(10). For convenience without losing generality, GPS L1 C/A, BDS B1C, and BDS B2a were selected as the representative signals in this article; their structures and characteristics are listed in Table 1.

More specifically, the pilot channel of the B1C signal with QMBOC(6,1,4/33) modulation consists of the BOC(1,1) modulated Pilot A and the BOC(6,1) modulated Pilot B components. Note that the Pilot A component of the B1C signal and the pilot channel of the B2a signal were utilized to get pseudorange measurements. Additionally, medium Earth orbit (MEO) signals instead of inclined

TABLE 1
Structures and Modulation Characteristics of Signals

Signal	Signal Components		Carrier Frequency (MHz)	Modulation		Phase	Power Ratio	Symbol Rate (sps)
GPS L1 C/A		$s_{L1CA}(t)$	1575.42	BPSK(1)		—	—	50
BDS B1C	data	$s_{B1C\_data}(t)$	1575.42	BOC(1, 1)		0	11/44	100
	pilot	$s_{B1C\_pilot\_a}(t)$		QMBOC(6, 1, 4/33)	BOC(1, 1)	90	29/44	0
		$s_{B1C\_pilot\_b}(t)$			BOC(6, 1)	0	4/44	
BDS B2a	data	$s_{B2a\_data}(t)$	1176.45	BPSK(10)		0	1/2	200
	pilot	$s_{B2a\_pilot}(t)$				90	1/2	0

geosynchronous orbit (IGSO) signals of BDS are designated for the generality of SBASs outside the Asian-Pacific region (e.g., WAAS and EGNOS).

2.2.2 | *EWF Modeling and its Space*

The performance of an SQM method is reflected by massive tests carried out on a maximized set of EWFs probably generated by a particular signal. This set is called the threat space (TS) of the signal. The need to specify TS makes our problem travel back to EWF modeling (i.e., the definition of the threat model [TM], which characterizes the approximate modeling forms of EWFs probably generated by the signal).

Several simple or complicated TMs were proposed to depict the bizarre behaviors in the SVN-19 Event but all were impractical or incomprehensible (Phelts, 2001). In 2000, the International Civil Aviation Association (ICAO) adopted a second-order step threat model (2OS-TM) in their *Standards and Recommended Practices* (SARPs), which divides the modeling modes of signal deformations into three categories (ICAO, 2006), namely digital (TM-A), analog (TM-B), and combined (TM-C) deformation modes. The TSs of GPS and GLONASS signals have been standardized in ICAO SARPs (ICAO, 2006). There have also been some discussions on the determination of the TM and TS of BOC(1,1) modulated signals. Fontanella (2010) established principles for EWF parameters, such as the absolute value of digital distortions not exceeding the length of the sub-chip, the value of damped natural frequencies being greater than the sub-chip rate, and damping factors not being too large in the case of over distortion. Further for TM-A, Sun (2016) categorized digital failures into three classes: pseudorandom noise (PRN) code generation failure, BOC(1,1) sub-carrier generation failure, and square wave composition failure.

For the unknowability of actual signal generating conditions, Pagot (2016) more realistically reduced TM-A to scenarios of modulated square waves. Partially supporting the reduction above, Wei (2020) proved that distortions in the Pilot B signal could not affect code tracking. In agreement with Pagot (2016), Cui (2020) used biases of all the modulated falling edges to model TM-A. There was not much argument about the definition of TM-B, nor of that of TM-C. To summarize, considering the fact that the BOC modulated signal generating hardware also consists of digital and analog components, the framework of 2OS-TM is adaptive to emerging signals for its maturity, simplicity, and wide applicability (Cui, 2020). TMs and TSs of Galileo (Selmi, 2020) and BDS (Cui, 2020) signals have been submitted to ICAO, respectively, and will soon be admitted into SARPs. The TSs of the three representative signals are listed in Table 2.

2.2.3 | *Constraints on Receiver Configurations*

Receiver configurations might have effects on both ranging and signal domains. In compliance with the specifications of ICAO (2018), reference receiver configuration and URCS in this paper are introduced in Table 3, in which the mixed Butterworth filter has the same amplitude response as sixth-order Butterworth and a 0-nanoseconds differential group delay. The four types of resonator filters are with a 24/30 dB per octave gain roll-off and a 0/150 nanoseconds differential group delay, respectively.

TABLE 2
Threat Spaces of Representative Signals

Signal	Threat Model	Δ (Chips)	f_d (MHz)	σ (MNp/s)
GPS L1 C/A	TM-A	–0.12 – 0.12	—	—
	TM-B	—	4 – 17	0.8 – 8.8
	TM-C	–0.12 – 0.12	7.3 – 13	0.8 – 8.8
BDS B1C	TM-A	–0.05 – 0.05	—	—
	TM-B	—	1.5 – 18	0.1 – 20
	TM-C	–0.05 – 0.05	1.5 – 18	0.1 – 20
BDS B2a	TM-A	–0.5 – 0.5	—	—
	TM-B	—	4 – 18	0.1 – 18
	TM-C	–0.5 – 0.5	4 – 18	0.1 – 18

TABLE 3
Reference Receiver Configuration and URCS

Receiver		Reference	User
Tracking	**L1 C/A**	E-L (BPSK(1) local replica)	
	B1C	E-L (BOC(1,1) local replica)	
	B2a	E-L (BPSK(10) local replica)	
Correlator Spacing	**L1 C/A**	0.10 chips	0.08, 0.10, 0.12 chips
	B1C		
	B2a	1.0 chips	0.9, 1.0, 1.1 chips
PCBw (double-sided)		24 MHz	12, 14, 16, 18, 20, 22, 24 MHz
Filter		sixth-order Butterworth	(1) sixth-order Butterworth (2) mixed Butterworth (3–6) four resonators

SQM systems are run on reference monitors, but the constraints on both the reference and the user receiver configurations will have an effect on the performance of the SQM method reflected in the ranging domain.

2.2.4 | *Performance Criteria in the Ranging Domain*

Three progressive concepts are defined in the ranging domain to embody the criteria of SQM performance:

1. **maxPRE** is the abbreviation for the *maximum differential pseudorange error*, being the maximum of the differential pseudorange errors obtained between the reference receiver and each specified user receiver within URCS toward a particular signal.
2. **MUDE** is the abbreviation for the *maximum undetected differential error*, as it is the maximum of the maxPREs obtained from all possible signals that are not asserted anomalous by SQM.
3. **MERR** is the abbreviation for the *maximum error range residual*, which is the maxPRE value obtained with the worst satellite geometries without resulting an HMI to users.

MERR is one concept of differential ranging error, defined more in-depth by ICAO (2006) as:

$$\mathrm{MERR} = K_{\mathrm{V,PA}} \cdot \sqrt{\sigma_{i,\mathrm{UDRE}}^2 + \min\left\{\sigma_{i,\mathrm{UIRE}}^2\right\}} \tag{1.1}$$

where $K_{\mathrm{V,PA}} \approx 5.33$ is a multiplier for the vertical direction of precision approach, $\sigma_{i,\mathrm{UDRE}}$ is the standard deviation of the user differential ranging error (UDRE) of satellite i, and $\sigma_{i,\mathrm{UIRE}}$ is the standard deviation of user ionospheric ranging error (UIRE) of satellite i (ICAO, 2006). Since the first-order ionospheric delay is eliminated, the dual-frequency MERR becomes:

$$\mathrm{MERR}_{\mathrm{DF}} = 5.33 \cdot \sigma_{i,\mathrm{DFRE}} \tag{1.2}$$

where $\sigma_{i,\mathrm{DFRE}}$ is the standard deviation of the dual-frequency ranging error (DFRE) of satellite i. If the MUDE exceeds the MERR, the effectiveness of an SQM algorithm should be denied.

In accordance with Phelts (2003, 2013), a UDRE Index (UDREI) value of 4 is the minimum provided by the WAAS conventionally. Since the DFMC SBAS is under standardization, in this paper, 4 is also selected as the minimum DFRE Index (DFREI) provided by the DFMC SBAS. Corresponding to the DFREI value of 4, dual-frequency MERR would be as small as 3.64 meters. Correspondences among UDREI/DFREI, L1-MERR, and DF-MERR are provided in Phelts (2013). As a consequence, the MERRs of each single frequency are given by:

$$\begin{cases} \mathrm{MERR}_{\mathrm{L1/B1}} = 3.64_{\mathrm{DFREI}=4} \Big/ 2.26_{\mathrm{L1/L5}} \approx 1.61 \text{ meters} \\ \mathrm{MERR}_{\mathrm{L5/B2}} = 3.64_{\mathrm{DFREI}=4} \Big/ 1.26_{\mathrm{L1/L5}} \approx 2.89 \text{ meters} \end{cases} \tag{2}$$

where the divisors of 2.26 and 1.26 are the error-inflating factors introduced by ionospheric-free combinations of L1/L5 dual-frequency.

The performance criteria for differential corrections in the ranging domain (i.e., MERRs) can be mapped to the requirements on the signal domain where SQM detections perform. Thus, for a subset of the specified TS, which consists of those EWFs whose maxPREs exceed a given MERR, if all of the included EWFs were detected, the performance of the SQM method would be approved.

To summarize, the overall objective of an SQM method is to guarantee that the MUDE from the given TM, TS, and receiver constraints does not exceed a specified MERR value under particular integrity requirement (Pagot, 2018). In later sections, we will propose a design methodology of a CDO-based SQM technique, along with assessments and a demonstration of simplification.

3 | OVERVIEWS OF CDO-BASED SQM AND ITS DESIGN METHODOLOGY

The design of an operational SQM method is affected by both the conceived SQM operation mode and the performance requirements of the protected application scenario. Section 3.1 describes an operation mode of the CDO-based SQM method in which all the influential factors worth considering are extracted and focused on. Meanwhile, the performance requirements (e.g., the probabilities of false-alarm and miss-detection in the signal domain and the MERR in the ranging domain) put forward constraints for the to-be-designed influential factors in order to make

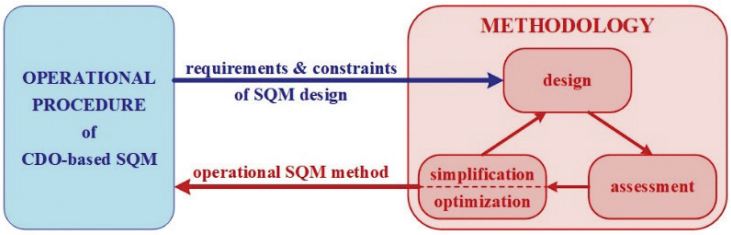

FIGURE 2 Overall logical relationships of operational SQM and its design methodology

SQM performance satisfactory. Section 3.2 introduces a design methodology and an ancillary verification platform based on the objective influential factors and the specified performance requirements. Additionally, an operational SQM method should be demonstrated after some possibly necessary iterations of design, assessment, and adjustment. The relationships among the modules of SQM design are shown in Figure 2.

3.1 | Operation Mode of the CDO-Based SQM Method

CDO measurements, on which metrics definition and thresholds estimation are based, are fundamental to SQM. A whole operational mode of the CDO-based SQM method is introduced in this section as a guidance to the proposed design methodology.

3.1.1 | Measurement of Raw CDOs

Raw CDOs are measured when tracking loops are locked and the carrier wipeoff process is performed. During conventional measurement, each individual chip is segmented into M bins with equal length in terms of implementation simplicity. Note that the code-phase bin lengths do not have to be equal. Then, M raw CDOs are obtained, each of which is physically an averaged measurement of the digitized sample points within the corresponding bin across a given integration period (Thevenon, 2014), expressed by:

$$\mathrm{CDO}_{i,raw} = \frac{1}{N_{\mathrm{bin}_i}^{\mathrm{samp}}} \cdot \sum_{j=1}^{N_{\mathrm{bin}_i}^{\mathrm{samp}}} \mathrm{SP}(j),\ 1 \le i \le M \tag{3}$$

where $N_{\mathrm{bin}_i}^{\mathrm{samp}}$ is the number of digitized sample points collected by bin_i within the specified integration period and $\mathrm{SP}(j)$ represents one sample point value. In terms of the AWGN assumption (Thevenon, 2014), the signal-to-noise ratio (SNR) of a raw CDO is accounted for by the number of digitized sample points participating in the averaging process. For better clarity, details of $N_{\mathrm{bin}_i}^{\mathrm{samp}}$ are given in Appendix A. In this phase, four out of the ten influential factors presented in Table 4 are incorporated:

- the integration period, T_{int}
- the proportion of a code-phase bin to a chip, BIN
- the sampling frequency of RF front-end output, F_S
- the double-sided PCBw, BW

3.1.2 | CDO Normalization

When an incoming navigation signal is steadily tracked by the monitoring receiver, a set of M raw CDOs and a raw in-phase component of the prompt correlator value, $I_{P,raw}$, are consecutively output at each monitoring epoch. θ_k is the elevation angle of epoch k. Normalizing processes also run at the current epoch, resulting in a set of M normalized CDOs, given by:

$$\mathrm{CDO}_{i,nml}(k) = \frac{\mathrm{CDO}_{i,raw}(k)}{I_{P,raw}(k)},\ 1 \le i \le M \tag{4}$$

This normalization process can eliminate the impact of unremoved navigation bits on the signs of raw CDOs and $I_{P,raw}$. In this phase, the fifth of the ten influential factors in Table 4 is the raw signal amplitude estimate, $I_{P,raw}$.

3.1.3 | Definition of Detection Metrics

The magnitudes of signal distortions reflected by CDOs toward detection metrics should be the prime concern in metric definitions. Here are three empirical rules for selecting CDOs to form metrics:

1. The CDOs applied to form metrics should be those measured near chip transitions. Recall that 2OS-TM is defined on chip transitions (e.g., TM-A on falling edges and TM-B on both rising and falling edges). Thus, the CDOs near a chip transition are intuitively more sensitive to deformations.
2. A designed SQM algorithm should be evaluated with a TM, conventionally. Under the current generic 2OS-TM, the CDOs near falling edges are not suitable for metrics because the evaluation of the designed SQM algorithm would be deceived by the dominant digital distortions due to the TM-A definition. Especially in TM-C, the potential analog distortions in falling edges would be concealed, introducing an uncertainty of fake sensitivities of these CDOs.
3. The CDOs near rising edges are suitable for metrics. All three EWF parameters in Table 2 can affect the total group delay differently. Consequently, although TM-A is not defined on rising edges, the analog distortion is not dominant there because the generated EWF with digital distortion would affect the total group delay to participate in determining code-phase bin segmentation and CDO calculation.

Therefore, CDOs on rising edges should be utilized in metric definitions according to Phelts (2013) and Wang (2021a). M CDOs should be measured across the rising edge (e.g., by putting the rising edge at or near the center). Wang (2021a) proposed a concept named the Rising Edge Rate (RER) that is PRN dependent. In this phase, the sixth of the ten influential factors in Table 4 is, thus, the RER—the ratio from the quantity of rising edges to that of chips within one code period.

Based on intentional design, N raw metrics are obtained by utilizing various elementary combinations of the M normalized CDOs at the current epoch (values and/or squares of individual CDOs, sums, differences, and/or products of CDO pairs, etc.).

3.1.4 | Metric-Smoothing Process

To further mitigate poorly temporally-correlated errors such as thermal noise and multipath (Pagot, 2016) on raw metric values beyond the given integral accumulation for each epoch, metric-smoothing processes are carried out by:

$$\text{metric}_{j,\,smt}^{\text{EWF}}(k)=\begin{cases}\dfrac{k-T_{\text{int}}}{k}\cdot\text{metric}_{j,\,smt}^{\text{EWF}}(k-1)+\dfrac{T_{\text{int}}}{k}\cdot\text{metric}_{j,\,raw}^{\text{EWF}}(k) & k\le T_{\text{smt}}\\ \dfrac{T_{\text{smt}}-T_{\text{int}}}{T_{\text{smt}}}\cdot\text{metric}_{j,\,smt}^{\text{EWF}}(k-1)+\dfrac{T_{\text{int}}}{T_{\text{smt}}}\cdot\text{metric}_{j,\,raw}^{\text{EWF}}(k) & k>T_{\text{smt}}\end{cases} \tag{5}$$

where $1\le j\le N$. Note that a variable time constant can be used within a period equal to the smoothing time constant after filter initialization in order to accelerate convergence (Xie, 2004). Then, a set of N smoothed metric values can be output at each epoch for detection. In this phase, the seventh of the ten influential factors in Table 4 is the metric-smoothing time constant, T_{smt}.

The metric-smoothing process can provide a site-dependent smoothing improvement factor (SIF) introduced in Section 3.2.1 and later detailed in Section 4.3.1.

3.1.5 | Determination of Nominal Metric Values and Thresholds

The determination of nominal metric values and thresholds is based on longtime observations and all such values are elevation dependent. The polynomial-fitting coefficients utilized to calculate nominal metric values and thresholds can be determined statistically by the Gaussian overbounding method (Xie, 2004) and then pre-stored. Given the elevation angle θ_k of the monitored satellite at epoch k, N nominal metric values and N thresholds can be calculated by applying these coefficients for SQM detection.

In operational SQM, a nominal metric value is given by the fitted mean value, $\mu_j(\theta_k)$, at a given elevation. The corresponding thresholds are a pair of the sum and the difference between $\mu_j(\theta_k)$ and a function of the fitted standard deviation, $\sigma_j(\theta_k)$, at the given elevation (Xie, 2004). They are given by:

$$\begin{cases}\text{metric}_j^{\text{nom}}(\theta_k)=\mu_j(\theta_k)\\ \text{Threshold}_j(\theta_k)=\mu_j(\theta_k)\pm K\cdot\sigma_j(\theta_k)\Big/\sqrt{N_{\text{ref}}}\end{cases} \tag{6}$$

where $1\le j\le N$ and K is a nominal scale multiplier given by application requirements. For an operational SQM system, K takes the value of K_{ffd}, where $K_{\text{ffd}}\approx 5.26$ for the probability of fault-free-detection lower than 1.5×10^{-7} per test by the Category I Precision Approach (CAT-I) requirement defined by ICAO (2006). For SQM design and assessment, however, K takes the value of the sum of K_{ffd} and K_{md}, where $K_{\text{md}}\approx 3.09$ for a probability of miss-detection lower than 1×10^{-3} per test (Phelts, 2001). To additionally improve SQM performance, a reference-smoothing process, which is a metric-averaging process across multiple in-view stations, is usually applied to mitigate poorly spatially-correlated errors such as multipath and/or non-spatially-correlated thermal noise. N_{ref} is the number of stations incorporated (Phelts, 2001).

Note that nominal metric values and thresholds are elevation dependent, while the elevation angle is positively correlated with the C/N_0 of the received signal. Thus, nominal metric values and thresholds are actually dependent on C/N_0. In this phase, the last three of our ten designated influential factors from Table 4 are incorporated:

- the nominal scale multiplier, K
- the minimum number of stations for reference-smoothing, N_{ref}
- σ-related carrier-to-noise ratio, C/N_0

3.1.6 | *Detection of SQM*

At each monitoring epoch, a figure of test (FoT) of the N tested metric values, which is the particular result for the test of a given epoch, is expressed by:

$$\text{FoT} = \max_{1 \le j \le N} \left\{ \frac{\left| \text{metric}_j^{\text{EWF}} - \text{metric}_j^{\text{nom}} \right|}{\text{Threshold}_j} \right\} \tag{7}$$

If $\text{FoT} \ge 1$, the monitored signal should be asserted anomalous.

Given the operational procedure of the CDO-based SQM method stated above, the ten designated influential factors of overall performance are observed. Classification, selections, derivations, and simulations of these factors constitute design methodology. These ten influential factors are summarized in Table 4.

TABLE 4
Influential Factors of SQM design

Algorithm phase	Influential Factor		
	Name	Symbol	Effect
Raw-CDO measurement	Integration period	T_{int}	Determines the total amount of chips, hence, bins in measuring a raw CDO
	Proportion of a code-phase bin to a chip	BIN	Determines the length of each bin, hence, the number of sample points probably incorporated by the measurement of a raw CDO
	Sampling frequency	F_S	Determines the density of sample points on chip waveforms
	Double-sided PCBw	BW	Determines the shape of chip waveforms, hence, the values of sample points and the shape of the correlation function (signal amplitude estimate)
CDO normalization	Signal amplitude estimate	I_P	Determines normalized magnitudes of CDOs
Metric definition	Rising edge rate	RER	Determines the total amount of rising edges within a given integration period in measuring CDOs applied to form metrics
Metric-smoothing	Metric-smoothing period	T_{smt}	Decreases the magnitudes of standard deviations of poorly temporally-correlated nominal errors
Determination of nominal metrics and detection thresholds	Nominal scale multiplier	K	Determines the inflated scales of nominal noise on metrics
	Minimum number of stations for reference-smoothing	N_{ref}	Decreases the magnitudes of standard deviations of poorly- and/or non-spatially-correlated nominal errors
	Carrier-to-noise ratio	C/N_0	Determines the raw magnitudes of nominal noise on received signals

Note that I_P is listed in Table 4 instead of $I_{P,\,raw}$ because the measured in-phase component of the prompt correlator value in simulations is always positive, without considering the unremoved navigation bits. Furthermore, I_P values of different PRNs are slightly different in simulations, as detailed in Section 4.

3.2 | Overview of Design Methodology for CDO-Based SQM

A general operational procedure of CDO-based SQM provides guidance for its specific design methodology under the framework of the DFMC model. The designed SQM method should be fully assessed and further design iterations with metric tests for simplification and/or optimization may be necessary. To cover the whole design process, the methodology of the proposed CDO-based SQM design is shown in Figure 3, including a more general macroscopic design flowchart in the upper yellow boxes in contrast to a microscopic design flowchart of the method within the large black dashed rectangle beneath it.

1. The design flowchart in the upper yellow region of the Figure 3 uses the SQM operational mode previously described as the input in which the designated influential factors incorporated are constrained by specific performance requirements and specifications (ICAO SARPs [ICAO, 2006], GNSS interface control documents [ICDs], DFMC standard drafts [ICAO, 2018], etc.). The shown design flow consists of some iterations of the SQM algorithm design and assessment for optimization and some potentially necessary metric tests for simplification. It finally outputs a robust CDO-based SQM method.
2. The elements outlined in the rest of Figure 3 highlighted in blue, orange, green, purple, and red mainly represent the designated influential factors. The ten factors are firstly classified into four categories: Specified, Dependent, Featured, and Smoothing-Related. These classifications are further described in Section 3.2.1. Six factors belonging to the Specified and Dependent categories can be obtained or calculated from the specifications, and two factors of the third category are associated with massive simulations based on the verification platform that is detailed in Section 3.2.2. Based on theoretical derivation, these eight factors are related to the minimum detectable errors (MDEs) introduced in Section 3.2.2 and further detailed in Section 4.1.2. The last two factors of the fourth category are treated as gain-contributors in simulations and discussed in Section 3.2.1. The output data for algorithm assessment is a configuration of the designed SQM algorithm, including the optimized bin and metric definition, along with the smoothing-related factors in which N_{ref} is conditioned by F_S.

3.2.1 | Influential Factor Classification

The 10 influential factors derived in Section 3.1 are classified into four categories, as listed below.

- **Specified** factors are fixed throughout the whole design process, including:
  - T_{int} representing the integration period: It conventionally equals 1 second in accordance with the temporal correlation of thermal noises.
  - BW representing the double-sided PCBw: It is set as 24 MHz in Table 3.
  - K representing the nominal scale multiplier: It is the sum of multipliers corresponding to the required probabilities of fault-free-detection and miss-detection.

- **Dependent** factors are conservatively determined and also fixed for corresponding representative signals, including:
  - I_P representing the signal amplitude estimate: It is no longer unity after filtering, but both signal- and PRN-dependent.
  - RER representing the rising edge rate: It is both signal- and PRN-dependent.
  - C/N_0 representing the carrier-to-noise ratio: This is signal-dependent—the theoretical minimum value for ground receivers that is calculated in accordance with the ICDs for conservativeness.

- **Featured** factors are relevant to SQM performance but not specified, so they must be designed. These include:
  - BIN representing the proportion of a code-phase bin to a chip: It is variable but better fixed in practical operations.
  - F_S representing sampling frequency: It is variable but better fixed in practical operations. It should be no lower than the Nyquist frequency, 24 MHz.

- **Smoothing-Related** factors are set for smoothing processes, including:
  - T_{smt} representing the metric-smoothing period: It equals 100 seconds for moving average filtering in steady-state SQM in accordance with the temporal correlation of multipath effects (Pagot, 2016) and time constant of airborne receivers standardized in SARPs (ICAO, 2006).
  - N_{ref} representing the minimum number of stations for reference-smoothing: This depends on the SNRs of CDOs, thus depending on the value(s) of F_S once all other factors have been determined.

Additionally, a concept of critical performance should be introduced, which is the detection performance of the raw metric values obtained at individual

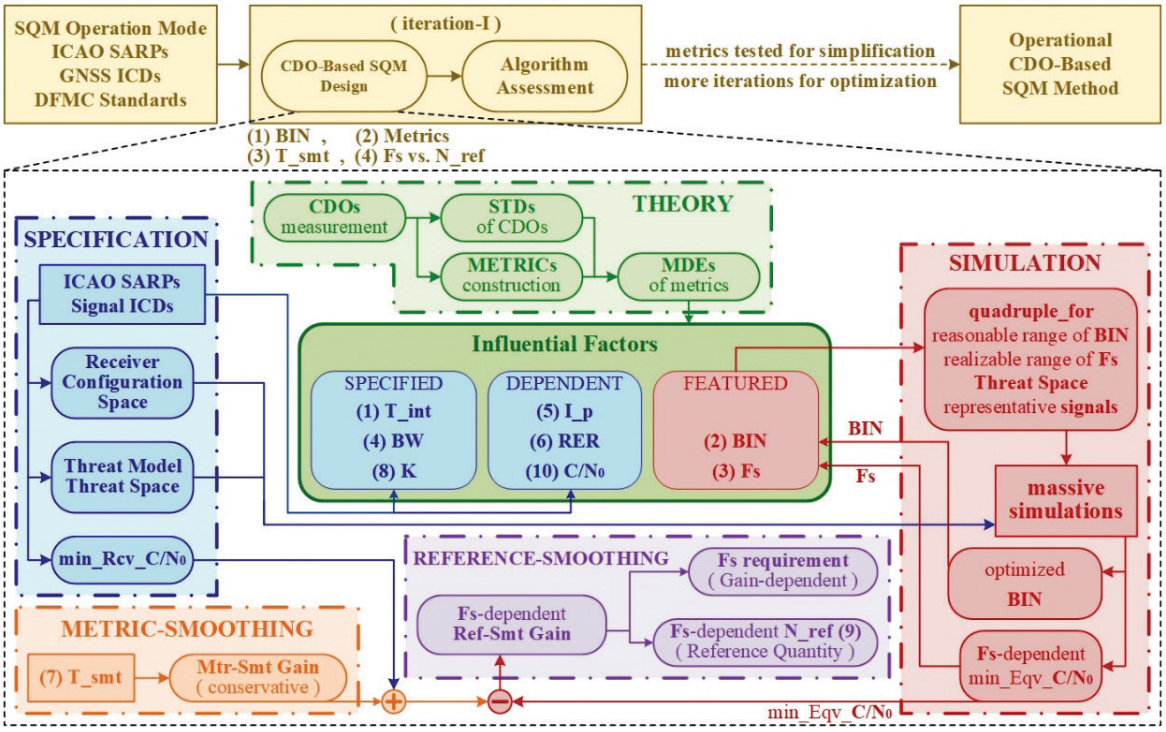

FIGURE 3 Design methodology of CDO-based SQM

epochs without smoothing processes throughout the TS. The process of metric measuring within a single integration period, T_{int}, and that of metric-smoothing across a given time constant, T_{smt}, are treated separately in the SQM design. The metric-smoothing process in steady state can simply be seen as a gain-contributor, providing a smoothing improvement factor (SIF) to be a denominator of the standard deviations of nominal noise on raw metric values under the Gaussian assumption (Pagot, 2018).

The reference-smoothing process behaves in a similar way. As a consequence, the influential factors related to critical performance are the eight factors belonging to the Specified, Dependent, and Featured categories. Further, according to the definitions, six of these eight factors can be obtained or calculated from official documents such as ICAO SARPs, GNSS ICDs, and DFMC standard drafts. Thus, the core factors to be designed for the critical performance of a CDO-based SQM algorithm are those of the Featured category (i.e., BIN and F_S). Before that, a reasonable range of BIN and a realizable range of F_S should be given; these are discussed in Section 4.2.1 and Section 4.2.2, respectively.

3.2.2 | *Introduction to the Verification Platform for SQM Design*

As indicated by the red rectangle flowchart in Figure 3 labeled *SIMULATION,* the verification platform plays a major role in algorithm design in which massive simulations are run. Two Featured factors that directly work on the critical performance are involved. Since the whole TS of each representative signal should be protected by the designed SQM method, any distorted signal from the discretized TS would be reversely utilized for algorithm design. Closed-form expressions of either nominal or deformed metric values, however, cannot be precisely derived using the given 2OS-TM formula in ICAO's SARPs (2006). Thanks to the progress of computing technology, this problem can be approximately solved by massive simulations with parallel computing.

Figure 4 illustrates the framework of the verification platform designed and applied for massive simulations of SQM design in this paper. For each one of the three representative signals, the procedure is described as follows:

1. **Signal level**: The whole process in Figure 4 is run for each particular one of the three representative signals. The simulations are carried out across the anomalous signals (EWFs) caused by corresponding reasonably discretized TSs.
2. **Channel level**: For each particular EWF point within the discretized TS, the distorted signal is processed by both the Reference Branch and the User Branch simultaneously:
   - At the Reference Branch, indicated by the color green, CDOs and metric values are obtained from the filtered chip waveforms and the reference pseudorange bias is measured from the correlation peak.
   - At the User Branch, indicated by the color red, a series of user pseudorange biases are measured across the specified URCS in Table 3.
3. **Calculation level**: Two examinations called Monitoring and Error Estimation, respectively, are incorporated here:
   - Monitoring is carried out in the signal domain on a dual-loop for the ranges of BIN and F_S. For any given combination of the two factors, the nominal and distorted CDO metric values and the MDEs are calculated to execute SQM detection as in Equation (6), resulting in an FoT that is then non-linearly

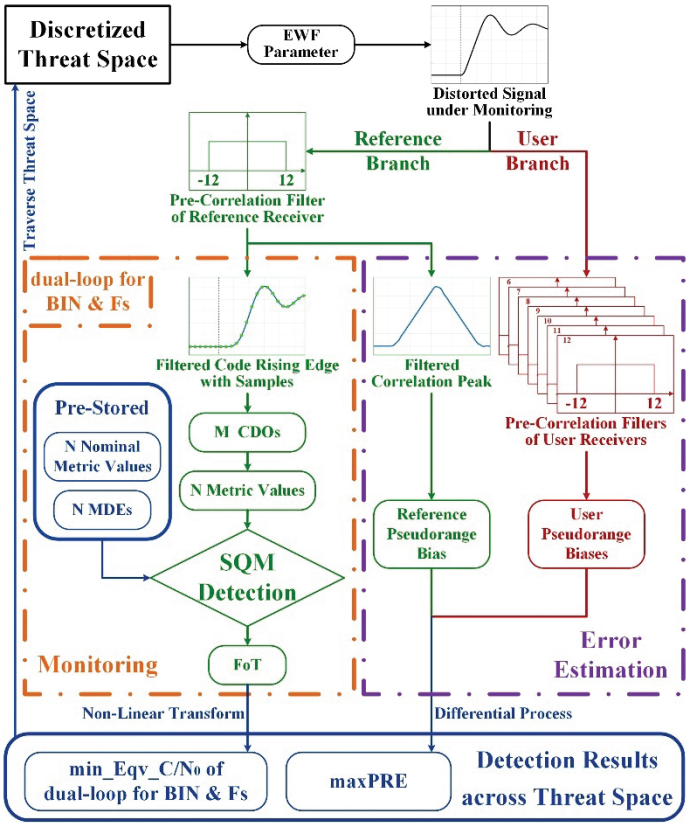

FIGURE 4 Framework of the verification platform for massive simulations of SQM design

transformed to a minimum equivalent C/N_0 (min_Eqv_C/N_0). An MDE is given by ICAO (2006) and repeated in Equation (8):

$$\mathrm{MDE}_j = \left(K_{\mathrm{ffd}} + K_{\mathrm{md}}\right) \cdot \sigma_j \tag{8}$$

where $1 \le j \le N$ and the standard deviations of the metrics, σ_j, are calculated with nominal signal at a theoretical minimum C/N_0 for ground receivers (min_Rcv_C/N_0) according to ICDs for conservativeness.

- Error Estimation is carried out in the ranging domain by converging the two branches (i.e., executing differential and sorting processes among reference and user pseudorange biases to obtain the maxPRE).

The performance of various configurations (i.e., BIN and F_S) are obtained via simulation across the discretized TS of a specific signal. Based on these results, an optimal BIN across various F_S can be derived. Further accounting for implementation generality, an optimized BIN across the three signals can be achieved.

With the provided BIN, a compromise between implementation complexity and diagnostic efficiency (i.e., sampling frequency and smoothing processes) would be made, supplementing enough gains for the required performance. Sufficient derivation, simulation, and assessment are detailed in later sections.

4 | DESIGN PROCESS OF CDO-BASED SQM

A detailed design for CDO-based SQM is demonstrated in this section based on the design methodology described in the last section. In accordance with the expressions of metrics and corresponding MDEs, the verification platform is

utilized in simulations to obtain critical performance of different algorithm configurations. An optimal BIN across the three representative signals is derived from analyses across contours. Furthermore, given a conservative gain of conventional metric-smoothing, the F_S-N_{ref} relationship is derived, resulting in a generic baseline algorithm of CDO-based SQM.

4.1 | Theoretical Expressions of Examining SQM Performance

4.1.1 | The Measurement of CDOs and Definition of Metrics

As the foundation of forming metrics, CDOs are obtained from various chip-waveform sections consecutively, as described in Equation (3). Based on the definitions of 2OS-TM by ICAO (2006), an anomalous signal distorted by an EWF of TM-B/C would oscillate violently after chip transitions. A damped oscillation might cause the difference between the distorted CDOs and their corresponding nominal values to vary significantly. On the other hand, given a fixed configuration of BIN and F_S, the EWFs with different damped oscillation frequencies and/or damping factors could result in different CDO values at the same corresponding code-phase bin. Referring to a NovAtel G-III monitor (Phelts, 2013) and the SCSQM8r algorithm (Wang, 2021a), we applied eight CDOs with rising edge symmetry (i.e., from CDO_1 to CDO_8 in time sequence uniformly with the rising edge between CDO_4 and CDO_5) to account for the sensitivity differences of different CDOs and EWFs.

Metric design is a key element of any SQM method. Metrics should be constructed to be as sensitive as possible utilizing different elementary combinations of CDOs. Since each CDO involves the information of limited sample points incorporated, it can reflect the baseline performance of a CDO-based SQM method by directly applying the CDOs, themselves, as metrics. Thus, to investigate the critical performance of the designed SQM algorithm, the eight metrics are defined as:

$$\text{metric}_{j,raw} = \text{CDO}_{j,nml},\ 1 \le j \le 8 \tag{9}$$

4.1.2 | MDEs in Detection

The high resolution of CDOs benefits from high sampling frequency of the RF front-end output (Thevenon, 2014). Basically, neither sampling frequency could be divided exactly by chip rate, nor were rising edges uniformly distributed in code sequence. If the condition of $F_S \cdot \text{BIN} \le \text{chip-rate}$ were strictly met, all sample points participating in the calculation of a raw CDO would come from different rising edges and would be considered independent of one other. On the other hand, chip sectionalization should not be too coarse (i.e., very few bins within a chip) in order to capture, instead of average, the violent oscillation sections. Simultaneously, the sampling frequency should not be too high in order to account for the implementation complexity, power consumption, and the correlation of sample points.

For the sake of the AWGN assumption of the RF front-end output (Thevenon, 2014), the eight metrics/CDOs have near-consistent standard deviations. Thus, the eight MDEs tend to be identical for a longer integral accumulation in operations. An equation for the approximate mean value of eight standard deviations of CDOs was given by Wang (2021a). This can be utilized to form the approximate mean value of the eight MDEs, which is detailed in Appendix A:

$$\overline{\mathrm{MDE}} \approx \frac{\left(K_{\mathrm{ffd}} + K_{\mathrm{md}}\right) \cdot BW}{I_P \cdot F_S \cdot \sqrt{2 \cdot T_{\mathrm{int}} \cdot \mathrm{RER} \cdot \mathrm{BIN}}} \cdot 10^{-\frac{C/N_0}{20}} \tag{10}$$

where eight out of the ten designated influential factors are incorporated for critical performance investigation, leaving the two factors related to smoothing processes to be tackled in Section 5.

The approximate mean value, $\overline{\mathrm{MDE}}$, is applied in later derivations and analyses for SQM design. In Equation (10), the three signal- and/or PRN-dependent influential factors (i.e., I_P, RER, and C/N_0) should be designated.

- Both I_P and RER are inconsistent across PRNs, where I_P is measured from a nominal correlation peak filtered by a sixth-order Butterworth filter with an E-L discriminator of 0.10-chip spacing and RER is obtained using the PRN code definition. Specifically, $\overline{\mathrm{MDE}}$ and $I_P \cdot \sqrt{\mathrm{RER}}$ are negatively correlated as indicated in Equation (10). Thus, the minimum values of $I_P \cdot \sqrt{\mathrm{RER}}$ (dimensionless) across all the PRNs in the shaded cells of Table 5 were chosen in theoretical analyses for conservativeness.
- The theoretical minimum value of each representative signal for ground receivers is conservatively taken by C/N_0, which is calculated in accordance with ICD specifications.

In particular, we should note that several situations were considered for the B2a signal. We intended to obtain a generally optimal BIN across the three representative signals, which is unknown before simulations and analyses. Thus, BINs within a reasonable range were tested. Conventionally, a rising edge can be expressed by the single-chip (−1, +1) situation. Since the length of an L5 chip is one-tenth of that of an L1 chip, if a tested BIN is larger than 1/40 of an L1 chip, the length of four bins would exceed the unity length of an L5 chip. On this account, the dual-chip (−1, −1, +1, +1) situation is applicable, in which two consecutive +1 chips are needed to cover the four late bins after the prompt point of a rising edge, and two consecutive −1 chips are needed for the four early bins similarly. Moreover, if a tested BIN is larger than 2/40 of an L1 chip, the triple-chip (−1, −1, −1, +1, +1, +1) situation would be applicable, and so on.

TABLE 5
Characteristics of Signals and PRN Codes

Signal	Min_Rcv_C/N$_0$ (dB-Hz)	Total PRN	Parameter		Mean	Median	Maximum	Minimum
GPS L1 C/A	39	32	$I_P^{\mathrm{L1CA}} \cdot \sqrt{\mathrm{RER}^{\mathrm{L1CA}}}$		0.4944	0.4959	0.5108	**0.4804**
BDS B1C (MEO)	37.5	63	$I_P^{\mathrm{B1C}} \cdot \sqrt{\mathrm{RER}^{\mathrm{B1C}}}$		0.8432	0.8431	0.8458	**0.8409**
BDS B2a (MEO)	39.3	63	$I_P^{\mathrm{B2a}} \cdot \sqrt{\mathrm{RER}^{\mathrm{B2a}}}$	single-chip (−1, +1)	0.4552	0.4550	0.4586	**0.4511**
				dual-chip (−1, −1, +1, +1)	0.2271	0.2271	0.2344	**0.2199**
				triple-chip (−1, −1, −1, +1, +1, +1)	0.1133	0.1125	0.1234	**0.1025**
				quad-chip (−1, −1, −1, −1, +1, +1, +1, +1)				

Provided all the specified and the signal/PRN-dependent factors, BIN and F_S are the only ones left to influence $\overline{\text{MDE}}$ for critical performance analyses of the reference monitor. Moreover, Equation (10) can be rewritten into a constant form, given by:

$$\overline{\text{MDE}} \cdot F_S \cdot \sqrt{\text{BIN}} = C_{\text{metric}} \tag{11}$$

where:

$$C_{\text{metric}} = \frac{\left(K_{\text{ffd}} + K_{\text{md}}\right) \cdot BW}{I_P \cdot \sqrt{2 \cdot T_{\text{int}} \cdot \text{RER}}} \cdot 10^{-\frac{C/N_0}{20}}$$

4.1.3 | *Eigen Properties Definition for Performance Analysis*

For the discretized TS of a representative signal, there must be many EWF points with corresponding maxPRE values larger than the specified MERR with the given receiver configuration spaces. These risky EWF points can be drawn out from the TS to form a risky group as an eigen subset. Only under the circumstances that all risky EWF points within the risky group are detected (i.e., resulting in a MUDE lower than the MERR) could the effectiveness of an SQM system be assessed as valid.

Given a configuration of BIN and F_S, there would be eight biases obtained by subtracting nominal metric values from distorted ones for each EWF point within the risky group. Then, the maximum of the eight biases can be obtained. Across all the risky EWF points, the minimum of all the maximums is defined as the critical metric bias (CMB) of the risky group, given by:

$$\text{CMB}_{\text{BIN, F}_\text{S}} = \min_{\text{RiskyGroup}} \left\{ \left[\max_{1 \le i \le 8} \left\{ \left| \text{metric}_i^{\left(\Delta, f_d, \sigma\right)} - \text{metric}_i^{\text{nom}} \right| \right\} \right]_{\text{BIN, F}_\text{S}} \right\} \tag{12}$$

A CMB value is eigen for a given configuration of BIN and F_S. It is necessary to make sure that the CMB value is higher than the corresponding $\overline{\text{MDE}}_{\text{BIN, F}_\text{S}}$, such that all risky EWF points can be detected.

In accordance with the definitions, a risky group and, hence, the CMB value are both MERR-dependent. Figure 5 gives a diagram of the risky group and CMB provider of the BDS B1C signal, where $F_S = 72$ MHz and $\text{BIN} = 0.025$ L1 chips were applied. Each of the blue scatters represents the detection result of an EWF point of the discretized TS, where the points to the left of the green vertical dashed line $\text{FoT} = 1$ would not be detected without smoothing processes, theoretically. The risky group consists of all the points beyond the specified MERR. Thus, the risky points are those not only with a $\text{FoT} < 1$ but also within the risky group, among which the CMB provider is exactly the one on the far left (i.e., the hardest to detect).

Furthermore, an index based on the figure of merit (FoM) is defined to examine the relationship between $\text{CMB}_{\text{BIN, F}_\text{S}}$ and the corresponding $\overline{\text{MDE}}_{\text{BIN, F}_\text{S}}$, given by:

$$\begin{aligned} \text{FoM}_{\text{BIN, F}_\text{S}} &= \text{CMB}_{\text{BIN, F}_\text{S}} \Big/ \overline{\text{MDE}}_{\text{BIN, F}_\text{S}} \cdot \text{SIF}\left(T_{\text{smt}}\right) \cdot \sqrt{N_{\text{ref}}} \\ &= \text{CMB}_{\text{BIN, F}_\text{S}} \cdot \frac{F_S \cdot \sqrt{\text{BIN}}}{C_{\text{metric}}} \cdot \text{SIF}\left(T_{\text{smt}}\right) \cdot \sqrt{N_{\text{ref}}} \end{aligned} \tag{13}$$

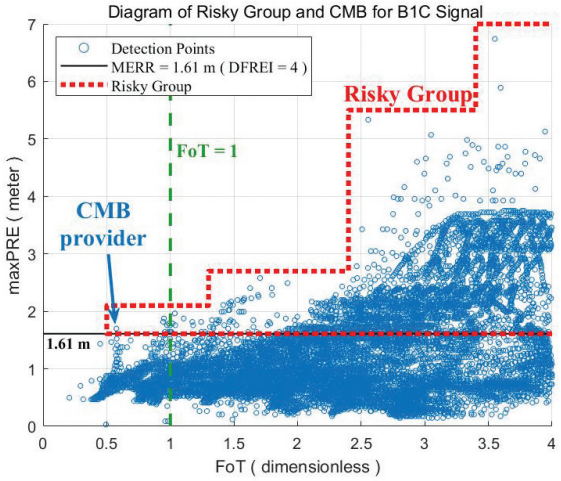

FIGURE 5 Diagram of risky group and CMB for BDS B1C signal

where the SIF is generally an increasing function of T_{smt} and reduces the standard deviations of metrics as well as the MDEs. The FoM value can be seen as a performance indicator of the designed SQM method (i.e., that the SQM is compliant with the considered requirements when $\text{FoM} > 1$).

In Equation (13), all 10 of the designated influential factors of Table 4 were incorporated explicitly. Furthermore, both BIN and F_S were also incorporated implicitly by $\text{CMB}_{\text{BIN, F}_S}$, which involves several aspects of uncertainties such as chip waveform distortions, irregularities in rising-edge distributions, and so on. Therefore, detailed investigation into the influences of both variables, BIN and F_S, were carried out with massive tests based on the verification platform in Figure 4.

4.2 | Determination of Optimal Code-Phase Bin Length

The measured CDOs represent a unique feature of the incoming chip waveforms. Conversely, the length of code-phase bins should have been able to allow the most significant features of the incoming chip-shape to be captured instead of averaged down by CDO measurements. A reverse derivation is described in this section, based on massive simulations across a reasonable range of BIN, a realizable range of F_S, a discretized TS, and three representative signals. This could transform the effectiveness of SQM (i.e., FoM values) to the effects across all the considered configurations of BIN and F_S.

4.2.1 | Empirical Constraints on Selection of Bin Length

Note that eight CDOs were obtained symmetrically about the rising edge. The four code-phase bins on each side should be neither too wide in the case of averaging down the oscillations of a potential EWF, nor too narrow in the case of missing the most violent oscillation. Therefore, constraints on the code-phase bin length are needed. In this section, an empirical method of constraint determination is given. Because of the 10-times relation between chip rates of dual-frequency signals, we utilized both L1 signals with lower chip rates in bin-length analyses without losing generality towards L5/E5/B2 signals.

Since we compare the differences of metric/CDO values between nominal and distorted signals against corresponding MDEs in detection, we must

TABLE 6
Constraints on Selection of Bin Length Based on L1 Signals

Domain	Constraint (chips)	Combined Constraint (chips)
Nominal	$4 \cdot \mathrm{BIN}_{\mathrm{nom}} > \Delta_1^{\mathrm{nom}}$ $\lceil 4 \times 68.27\% \rceil \cdot \mathrm{BIN}_{\mathrm{nom}} < \Delta_1^{\mathrm{nom}} + \Delta_2^{\mathrm{nom}}$	$0.0107 < \mathrm{BIN}_{\mathrm{nom}}^{\mathrm{L1}} < 0.0438$
Distorted	$4 \cdot \mathrm{BIN}_{\mathrm{EWF}} > \dfrac{\text{chip-rate}}{\max\{f_d\}}$ $\lceil 4 \times 68.27\% \rceil \cdot \mathrm{BIN}_{\mathrm{EWF}} < \dfrac{\text{chip-rate}}{\min\{f_d\}}$	$\begin{cases} 0.0150 < \mathrm{BIN}_{\mathrm{EWF}}^{\mathrm{L1C/A}} < 0.0853 \\ 0.0142 < \mathrm{BIN}_{\mathrm{EWF}}^{\mathrm{B1C}} < 0.2273 \end{cases}$
Rigid	$\begin{cases} 4 \cdot \mathrm{BIN}^{\mathrm{L1C/A}} < 1.0 \\ 4 \cdot \mathrm{BIN}^{\mathrm{B1C}} < 0.5 \end{cases}$	

also analyze the constraints on bin-length selection from both nominal and distorted signals.

- For nominal signals, two featured lengths in time domain Δ_1^{nom} and Δ_2^{nom} are defined, standing for the two segments with the fastest change on a rising edge, respectively. Thus, $\Delta_1^{\mathrm{nom}} \approx 0.0429$ chips and $\Delta_2^{\mathrm{nom}} \approx 0.0885$ chips are measured with a nominal chip waveform filtered by a sixth-order Butterworth filter, as detailed in Appendix B.
- For distorted signals, because of the induced EWF parameter of damped oscillation frequency, f_d, one featured length in time domain, $\Delta^{\mathrm{EWF}} = \text{chip-rate} / f_d$, is defined, varying with the range of f_d in Table 2.

Five constraints are listed in Table 6, where the 1σ percentage, 68.27%, was utilized to force the main portion of the four bins to capture the main part of the oscillating information without losing the sensitivities of a limited number of CDOs. The reason for using the 1σ percentage value is introduced in Appendix B. By intersecting the five constraints for both signals for generality, conciseness, and inter-consistency in an operational DFMC SBAS SQM design, the range of BIN for L1 signals is derived as:

$$0.0150 \text{ chips} < \mathrm{BIN}^{\mathrm{L1C/A,\,B1C}} < 0.0438 \text{ chips} \tag{14.1}$$

or in fractional form:

$$1/66 \text{ chips} \le \mathrm{BIN}^{\mathrm{L1C/A,\,B1C}} \le 1/23 \text{ chips} \tag{14.2}$$

For the BDS B2a signal, the much shorter chip duration makes it only capable of arranging eight finer bins under a single-chip (−1, +1) situation. As a consequence, longer situations are needed to arrange eight coarser bins to form a concatenation of sub-ranges to fulfill the range of Equation (14) indicated in Table 5. By splitting Equation (14.2) to adapt the B2a signal, the fraction-form constraints would be expressed by:

$$\begin{cases} \text{For single-chip}: 1/7 \text{ chips} \le \mathrm{BIN}^{\mathrm{B2a}} \le 1/4 \text{ chips} \\ \text{For dual-chip}: 2/7 \text{ chips} \le \mathrm{BIN}^{\mathrm{B2a}} \le 2/5 \text{ chips} \\ \text{For triple-chip}: 3/8 \text{ chips} \le \mathrm{BIN}^{\mathrm{B2a}} \le 3/7 \text{ chips} \end{cases} \tag{15}$$

For which the rigid constraints would be provided as:

$$\begin{cases} 4 \cdot \mathrm{BIN}^{\mathrm{B2a}}_{\text{single-chip}} \le 1.0 \text{ chip} \\ 4 \cdot \mathrm{BIN}^{\mathrm{B2a}}_{\text{dual-chip}} \le 2.0 \text{ chips} \\ 4 \cdot \mathrm{BIN}^{\mathrm{B2a}}_{\text{triple-chip}} \le 3.0 \text{ chips} \end{cases}$$

Even longer situations (e.g., quad-chip [−1, −1, −1, −1, +1, +1, +1, +1]) were not considered because the SNRs of their metrics would reduce sharply due to the approximately four-time decrease in RER values.

4.2.2 | *Determination of Generally Optimal BIN*

Provided the reasonable ranges of BIN, a realizable range of F_S is determined as follows:

- the lower bound is definitely given by the Nyquist frequency corresponding to the PCBw of the reference station; and
- the upper bound is valued as the minimum integer-times of single-sided PCBws to provide weakly correlated sample points participating in CDO calculations for the lower bound of the BIN-range for L1 signals (i.e., 1/66 L1 chips per bin).

To sum up, the range of F_S applied in simulations is between 24 MHz and 72 MHz.

Contours of FoM values beyond the two-dimensional plane of both BIN and F_S could be utilized to show the performances of various configurations. The FoM contours of the three representative signals are given in Figure 6 in which both SIF and N_{ref} are valued unity in analyzing the critical performance of individual monitors and the considered conservative C/N_0 values apply the min_Rcv_C/N$_0$ values from Table 5.

Figure 6(b) shows that the contours of the B1C signal are underneath unity in the worst case for conservativeness (i.e., there are always some risky EWF point[s] undetected under any configuration of BIN and F_S within the given ranges). While, for the L1 C/A signal in Figure 6(a), FoMs at 1/37 to 1/35 chips under 72-MHz sampling were beyond unity. For most of the contours in each figure, the FoMs would benefit from a lift of F_S at any fixed BIN corresponding to the expression in Equation (13). However, trends of the FoM contours with varying BIN values at a fixed F_S value would not be monotonic.

There is also a configuration-dependent variable in Equation (13): $\mathrm{CMB}_{\mathrm{BIN,F_S}}$, which is weakly correlated with F_S according to simulation results. Thus, a multiplier of $1/F_S$ was applied to the FoM contours to account for the effects of sampling frequencies in Equation (13), and both L1 signals were equally weighted. As a consequence, the optimal BIN (i.e., 1/40 chips) was observed. For the BDS B2a signal in Figure 6(c), contours were segmented by 0.25 and 0.4 chips-per-bin horizontally, as indicated in Equation (15). The best performances corresponded to 0.25 chips-per-bin identically.

In summary, a generally optimal code-phase bin length for dual-frequency signals is about 24.438 nanoseconds per bin (i.e., 1/40 L1 chips or 1/4 L5 chips-per-bin identically).

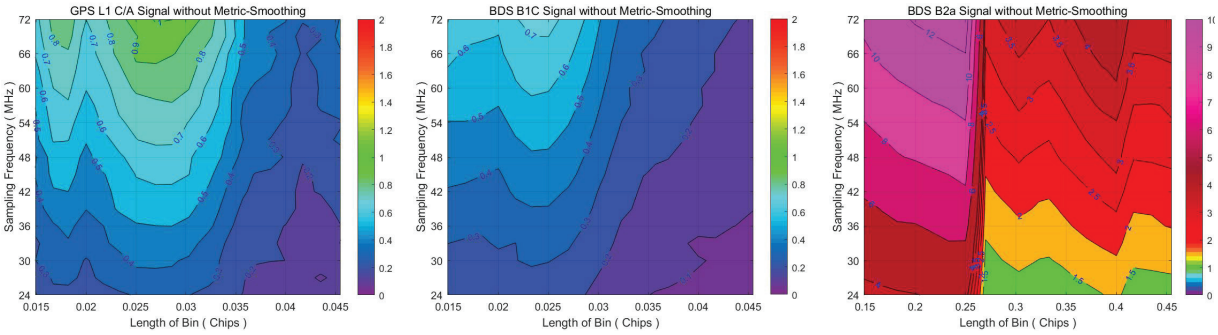

(a) GPS L1 C/A (b) BDS B1C (c) BDS B2a

FIGURE 6 FoM contours with 1-second integral accumulation only

4.3 | Conservative Scheme of Smoothing Processes

To mitigate the poorly temporally-correlated and/or poorly spatially-correlated errors on raw metric values beyond the given integral accumulation, metric-smoothing and reference-smoothing processes are needed because operational SQM performance would be augmented beyond the critical performance. In simulations, metric-smoothing is beneficial to FoM values by raising T_{smt}, thus improving the SIF to reduce MDEs, while reference-smoothing provides improvement by a multiplier of $\sqrt{N_{\text{ref}}}$ (Phelts, 2001). Thus, given the generally optimal BIN value, a higher F_S value might result in a shorter required smoothing constant and/or fewer required stations to improve SQM performance, but higher implementation complexity would also be induced.

This section aims to provide a demonstration of smoothing processes for steady-state, instead of transient, SQM design. In fact, the transient performance of an SQM method is evaluated for its ability of addressing the onset of an EWF event within the specified time-to-alarm (TTA) period, when neither the maxPRE nor the other metric values reach the final state (Phelts, 2001). Nevertheless, the transient SQM problem may be mitigated by adding more sensitive metrics (Phelts, 2001). More specifically, several important aspects (such as the different types, time constants, and initializing times of the smoothing filters for reference and user receivers, respectively, the times of EWF event onset or anomalous satellite acquired, etc.) are involved in this problem, which is out of the scope of this paper.

In this section, the last two smoothing-related influential factors (i.e., T_{smt} and N_{ref}) are discussed. Figure 6(c) shows that the B2a signal was well guaranteed across the considered range of F_S at the generally optimal BIN, whereas the situation is quite the opposite for both L1 signals, for which their smoothing processes are examined.

4.3.1 | *Effects of the Metric-Smoothing Process*

A metric-smoothing process was applied to reduce thermal noise and multipath effects, resulting in an enhanced performance—a lower min_Eqv_C/N_0 in demand—than that of individual epochs; in other words, it reduces the standard deviations of metrics (MDEs) to improve FoMs. The airborne receiver time constant of 100 seconds standardized in SARPs (Pagot, 2016) was applied as T_{smt}.

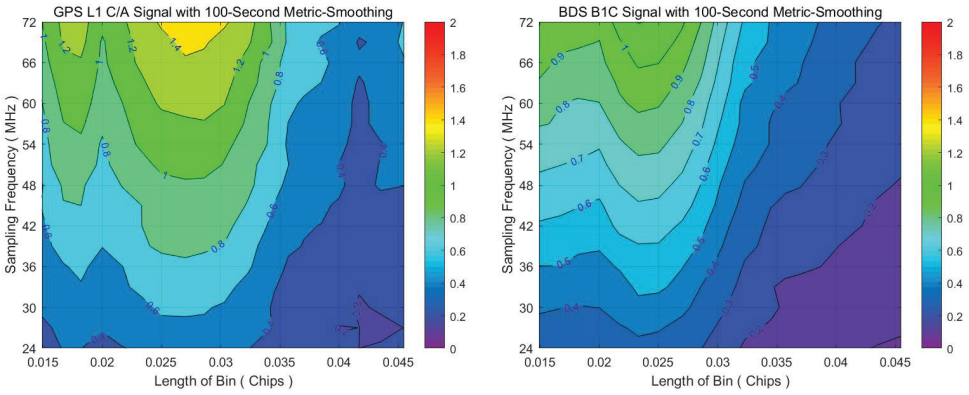

(a) GPS L1 C/A (b) BDS B1C

FIGURE 7 100-second metric-smoothing-improved FoM contours for individual station

For the conventional 100-second metric-smoothing process, a SIF is introduced at a value between 1.5 and 2.3 because of various multipath effects. To be conservative, 1.5 would be applied, which could provide a 4-dB gain in sensitivity (Pagot, 2018). Contours of smoothing-improved FoMs for both L1 signals are given in Figure 7 by setting $T_{\text{smt}} = 100$ seconds, hence $\text{SIF} = 1.5$ for individual station (i.e., $N_{\text{ref}} = 1$). Given the selected general optimal BIN value of 1/40 L1 chips at the horizontal axis, the lower half of the range of F_S in Figure 7(a) and most of that in Figure 7(b) could not provide a conservative enough performance to meet the requirement, hence reference-smoothing conditions would be needed under these circumstances.

4.3.2 | *Derivation of Reference-Smoothing Demands*

Reference smoothing is an averaging process incorporating several in-view stations (Phelts, 2001). It is required when metric-smoothing cannot conservatively guarantee the objective signal to meet integrity demands (i.e., a case in which some risky EWFs might evade SQM detection by pretending to be near-worst nominal signals). Please note that metric-smoothing is identical for all the reference stations, as is the considered conservative gain of metric-smoothing in SQM design. In practice, all the participating stations in reference-smoothing are beyond the worst observing conditions, validating all conservative assumptions for individual stations.

To improve FoM values at any given point with generally optimal BIN values, a family of station-dependent curves with different F_S values were developed to determine the minimum number of stations needed, which are shown in Figure 8(a) and Figure 8(b). Please note that the curve values at the bottom of Figure 8(a)—where the vertical axis is always taken as unity—are consistent with the contour values in the vertical direction with BIN = 0.025 chips in Figure 7(a). The same is true for the B1C signal in Figure 8(b).

The processes are similar in the best environment where SIF = 2.3. Table 7 provides the required N_{ref} values with various F_S values for the two extreme SIF values as a reference. Additionally, it can be seen that a better multipath environment is beneficial to yield a decrease in the number of required stations for reference smoothing.

Moreover, the curve values at the bottom of Figure 8(a) can be mapped to Figure 9, where the scattered points can be linearly fitted onto a straight line as well. By further combining the unity-crossing values in Figure 8(a) and the linear

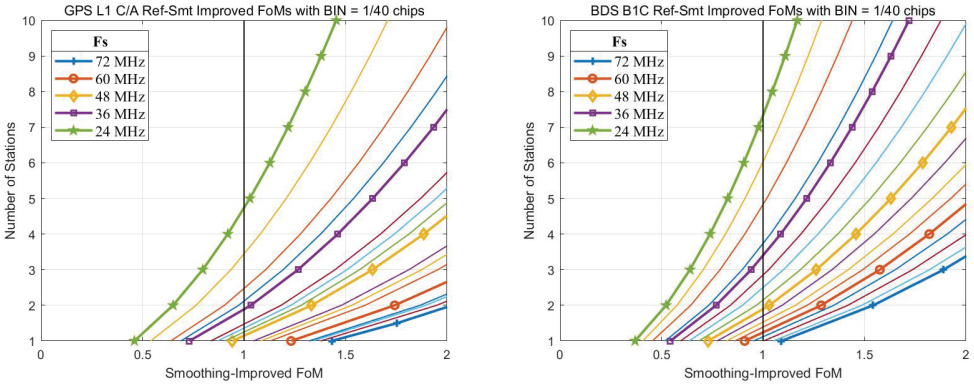

(a) GPS L1 C/A (b) BDS B1C

FIGURE 8 Reference-smoothing-improved FoM curves at BIN = 0.025 chips

TABLE 7
Number of Stations Needed for Various Sampling Frequencies

F_S (MHz)	N_{ref}			
	GPS L1 C/A		BDS B1C	
	SIF = 1.5	SIF = 2.3	SIF = 1.5	SIF = 2.3
72	1	1	1	1
66	1	1	1	1
60	1	1	2	1
54	1	1	2	1
48	2	1	2	1
42	2	1	3	2
36	2	1	4	2
30	3	2	5	3
24	5	3	8	4

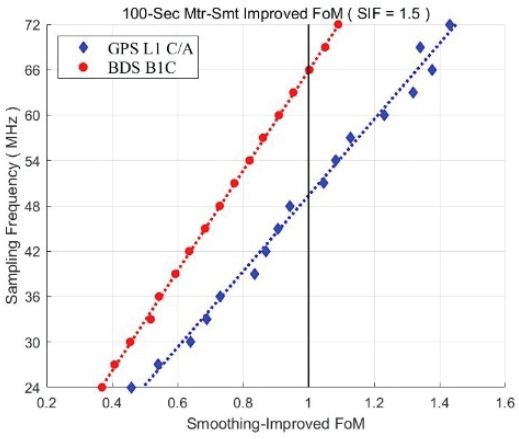

FIGURE 9 Improved FoMs for individual station at BIN = 0.025 chips

function in Figure 9, the F_S-N_{ref} relationship can be obtained. The same is true for the B1C signal.

Thus far, a baseline algorithm of CDO-based SQM with the proposed design methodology has been fulfilled and summarized in Table 9 at the end of Section 5.

5 | ASSESSMENT AND SIMPLIFICATION OF BASELINE ALGORITHM

A baseline algorithm of CDO-based SQM was designed, of which the correctness and effectiveness must be verified. Performance comparisons between the designed CDO-based and traditional MCO-based SQMs are discussed as well. Since the distortion magnitudes within different segments of the rising edge vary significantly, the detection ability of the metrics might be different as well. This property is utilized to form an example of algorithm simplification in order to complete the demonstration of the proposed design methodology.

5.1 | Assessment of Baseline Algorithm of CDO-Based SQM

The aim of the assessment is to determine whether the resultant required minimum equivalent C/N_0, which should guarantee an undetected portion of the TS with an MUDE lower than MERR, can be bounded by the combined condition of a theoretical minimum ground-receiving C/N_0 and the gains of smoothing processes. The derived F_S-N_{ref} relation is assessed first. Then, comparisons between the designed CDO-based and traditional MCO-based SQM methods are made. The TSs of the three representative signals are discretized as Table 8 does, noting that:

- The rising and falling edges of a filtered chip waveform is not centrosymmetric to the prompt point. The prompt points are not zero-crossing points of a filtered chip waveform, either. Thus, distortions caused by the negative halves of the TSs of TM-A and TM-C models could not be deemed symmetric to those by the positive halves. As a result, the whole TS must be applied.
- The TS of the B2a signal was enlarged to facilitate quantitative analysis, because distortions caused by EWFs precisely within the specified TS were not particularly noticeable for the rounding effect toward correlation peaks.

5.1.1 | Reference-Smoothing Condition Assessment

Three pairs of assessment examples of the baseline algorithm designed in the last section can be carried out with three representative signals, respectively. The procedure of the assessment is given by Figure 4 with fixed configurations of BIN

TABLE 8
Discretization Scheme of Threat Spaces

Signal	Threat Model	Δ (chips)	f_d (MHz)	σ (MNp/s)
GPS L1 C/A	TM-A	–0.12 : 0.01 : –0.01, 0.01 : 0.01 : 0.12	—	—
	TM-B	—	4 : 0.1 : 17	0.8 : 0.5 : 8.8
	TM-C	–0.12 : 0.01 : –0.01, 0.01 : 0.01 : 0.12	7.3 : 0.1 : 13	0.8 : 0.5 : 8.8
BDS B1C	TM-A	–0.05 : 0.01 : –0.01, 0.01 : 0.01 : 0.05	—	—
	TM-B	—	1.5 : 0.5 : 18	0.1, 0.5 : 0.5 : 20
	TM-C	–0.05 : 0.01 : –0.01, 0.01 : 0.01 : 0.05	1.5 : 0.5 : 18	0.1, 0.5 : 0.5 : 20
BDS B2a	TM-A	–0.9 : 0.1 : –0.1, 0.1 : 0.1 : 0.9	—	—
	TM-B	—	2 : 1 : 20	0.1, 1 : 1 : 20
	TM-C	–0.9 : 0.1 : –0.1, 0.1 : 0.1 : 0.9	2 : 1 : 20	0.1, 1 : 1 : 20

and F_S, and reference and user receivers apply the configurations from Table 3. Especially:

- F_S : 33 / 66 MHz for each signal
- Optimal BIN: 0.025 / 0.25 chips for L1 / L5 signals

Figure 10 gives the results of the six assessment examples. For the L1 C/A signal with an F_S value of 33 MHz in Figure 10(a), the following equation can be observed:

$$39\ \text{dB-Hz} + 4\ \text{dB} + 10 \cdot \log_{10} N_{\text{ref}} > 46.2\ \text{dB-Hz} \tag{16.1}$$

such that Min_Eqv_C/N_0 of 46.2 dB-Hz, which stands for the required minimum equivalent C/N_0, can be bounded conservatively by a combination of the theoretical minimum C/N_0 for ground receivers (39 dB-Hz), a 100-second metric-smoothing (4-dB gain) process, and a reference-smoothing process with three stations. Similarly, for the L1 C/A signal with an F_S value of 66 MHz in Figure 10(b), the following equation can be observed:

$$39\ \text{dB-Hz} + 4\ \text{dB} + 10 \cdot \log_{10} N_{\text{ref}} > 39.8\ \text{dB-Hz} \tag{16.2}$$

such that the Min_Eqv_C/N_0 value of 39.8 dB-Hz can be bounded conservatively by the theoretical 39 dB-Hz and the 4-dB metric-smoothing gain by a single station. Furthermore, by doubling the F_S value of 33 MHz to 66 MHz, the value of Min_Eqv_C/N_0 would sharply decrease by 6.4 dB-Hz—about twice the 3-dB gain provided by doubling the value of F_S. In other words, the 6.4-dB improvement in SQM performance can be accounted for by the sum of the 3-dB gain by doubling F_S and the 4.8-dB gain from triple-station smoothing. Similar results could be observed for the B1C signal with an F_S value of 33 MHz and 66 MHz in Figure 10(c) and 10(d), respectively:

$$37.5\ \text{dB-Hz} + 4\ \text{dB} + 10 \cdot \log_{10} N_{\text{ref}} > 46.8\ \text{dB-Hz} \tag{16.3}$$

$$37.5\ \text{dB-Hz} + 4\ \text{dB} + 10 \cdot \log_{10} N_{\text{ref}} > 41.1\ \text{dB-Hz} \tag{16.4}$$

For the B2a signal in Figure 10(e) and 10(f), the Min_Eqv_C/N_0 value was 24.0 dB-Hz and 17.8 dB-Hz, respectively—much lower than the theoretical minimum value. Thus, no smoothing process needed to be considered in the design, as indicated in Figure 6(c). More specifically, the critical performance of the B2a signal with any value of F_S no lower than 24 MHz could meet the requirements.

By carrying out a group of assessments, of which six examples were briefly introduced here (those for the L1 signals are listed in Appendix C), the designed baseline algorithm was validated.

5.1.2 | Performance Comparisons Between Designed CDO-Based and Traditional MCO-Based SQMs

Traditional multi-correlator-based SQM methods for the three representative signals have been well described by Phelts (2001), Wei (2020), and Wang (2021b), respectively. Since all the sample points of the RF front-end output were utilized to form the local cross-correlation function in which the MCOs are measured to

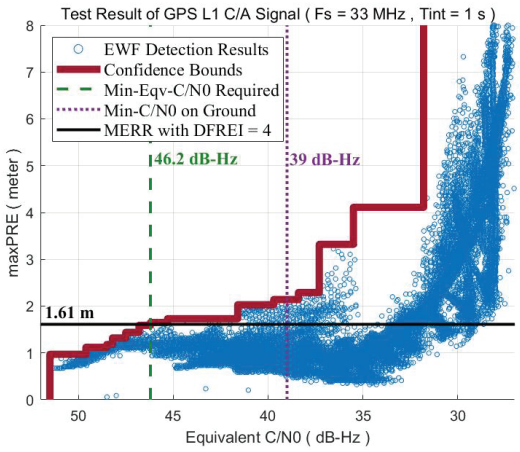

(a) 33 MHz Sampling on GPS L1 C/A

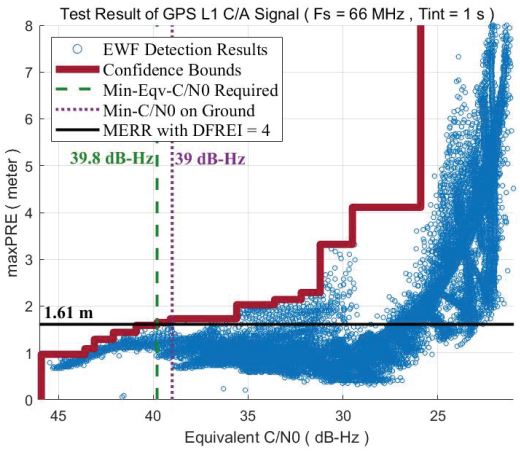

(b) 66 MHz Sampling on GPS L1 C/A

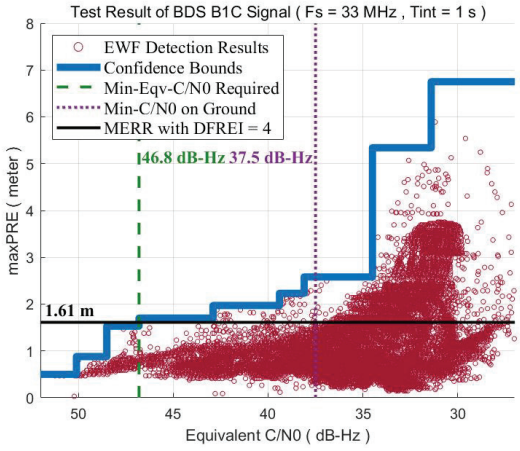

(c) 33 MHz Sampling on BDS B1C

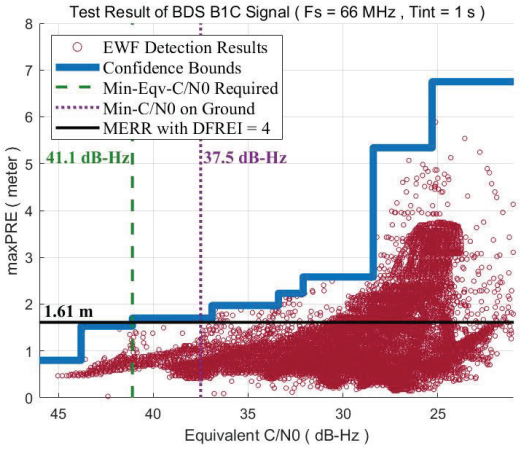

(d) 66 MHz Sampling on BDS B1C

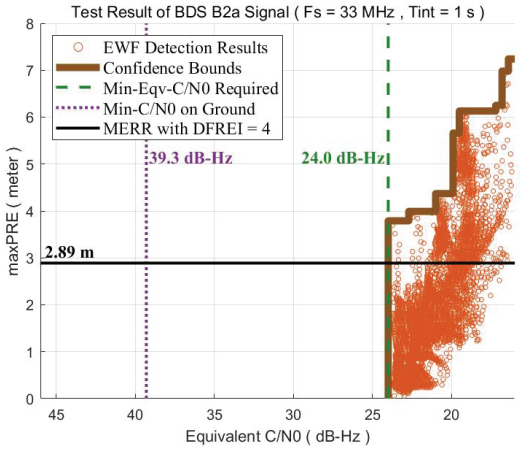

(e) 33 MHz Sampling on BDS B2a

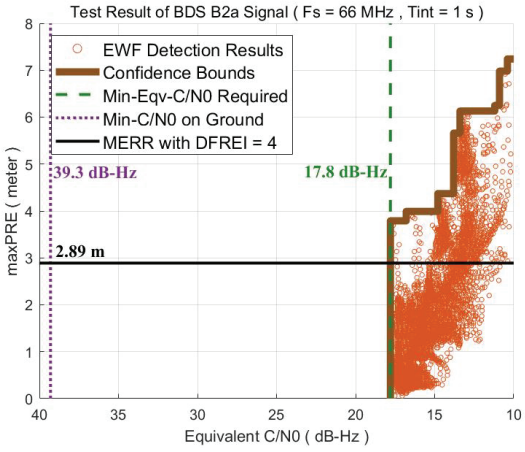

(f) 66 MHz Sampling on BDS B2a

FIGURE 10 Results of assessment examples

compute metric values, the performance of an MCO-based SQM method could be considered to be sampling independent. On the contrary, provided with a fixed optimal bin length, the SNRs of the resulting CDOs would be strongly dependent on the quantities of sample points collected by the bins. In other words, the performance of a CDO-based SQM method is sampling dependent.

For performance comparison, simulations of traditional MCO-based SQM were carried out with the three signals. 51 correlators were uniformly distributed from −0.25 to +0.25 chips for both L1 signals, and 21 correlators were from −1.0 to +1.0 chips for the B2a signal. The metrics were defined as:

$$\begin{cases} M_{\text{simple}} \equiv I_x / I_{\text{P}} \\ M_{\text{diff}} \equiv \left(I_{-x} - I_x\right) / I_{\text{P}} \\ M_{\text{sum}} \equiv \left(I_{-x} + I_x\right) / I_{\text{P}} \end{cases} \tag{17}$$

where I_x is the in-phase component of an E-L correlator value, and I_{P} is that of the prompt correlator value. Pagot (2018) stated that the approximate best detection performance of an MCO-based SQM algorithm could be reached by applying these metrics.

Figure 11 shows critical performance comparisons between the traditional MCO-based SQM method and the proposed CDO-based SQM method using simulations. The diamonds in blue (G1) represent the performance of the CDO-based methods with the L1 C/A signal, as well as the dots in red (C1) and the stars in orange (A1) for those performances with the B1C and B2a signals, respectively. Correspondingly, the indigo (G2), maroon (C2), and brown (A2) dashed vertical lines represent the performance of the MCO-based method, respectively. The performances of the CDO-based method with the L1 C/A signal were superior to that of the MCO-based method from the very beginning of 24-MHz sampling. However, those performances with the B1C and B2a signals needed an F_S value of no lower than 33 MHz and 39 MHz (rounded up) to surpass the MCO-based performances, respectively. The Min_Eqv_C/N_0 for either the MCO- or the CDO-based method with the B2a signal was much lower than the theoretical receiving value, allowing for satisfactory performance with an F_S value as low as 24 MHz.

In practice, the F_S of the RF front-end output were identical to the concurrently monitored signals. In order to achieve better performance than that of the

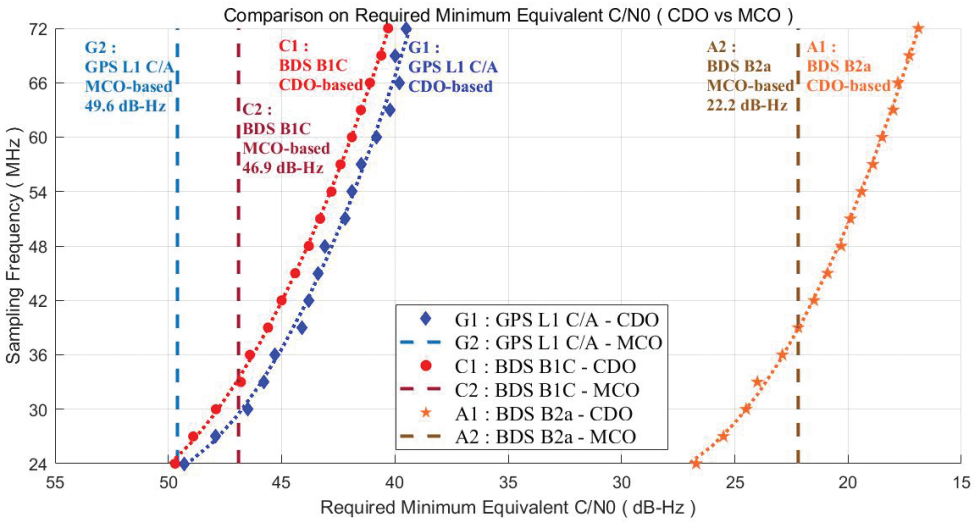

FIGURE 11 Critical performance comparisons with three signals

traditional MCO-based method, the F_S value of the CDO-based SQM for DFMC SBAS was suggested to be no lower than 33 MHz. An F_S lift could certainly provide an improvement in the critical performance, as indicated in Figure 11. However, as the F_S value increases, the marginal gain of an F_S lift for the critical performance decreases. Additional implementation complexity as well as correlations of sample points are also induced. The quantitative relationship between an F_S lift and the corresponding gain in the critical performance is given as:

$$\frac{\left[F_S\right]_2}{\left[F_S\right]_1} \cdot 10^{\frac{\left[\text{Min\_Eqv\_C/N}_0\right]_2 - \left[\text{Min\_Eqv\_C/N}_0\right]_1}{20}} \approx 1.0 \tag{18}$$

Thus, given the optimal BIN value, the upper bound of the critical performance was ultimately determined by the implementation of the RF front-end output sampling. One step further, BIN and F_S are the real determinants of the critical performance of a CDO-based SQM method.

5.2 | Simplification of the Baseline Algorithm

Numerous differently defined metrics were formed in the first design iteration as candidates, introducing computation complexity. Thus, simplification to a designed baseline algorithm would certainly be needed. The sensitivities of the metrics were inconsistent because of the damped oscillations as defined by 2OS-TM. Note that the eight CDOs were directly applied as eight metrics in this article. By checking the sensitivities of these metrics/CDOs in this section, a demonstration of simplification was proposed for the baseline algorithm designed and validated above.

Figure 12(a) gives the result of critical performance for an individual monitor with an F_S value of 72 MHz. The most sensitive CDOs for the three signals were CDO-5 and/or CDO-4. For both L1 signals, the second most sensitive signal was CDO-8, identically. While for the B2a signal, it could be any one of the rest. Furthermore, even with an F_S value as high as 72 MHz, the critical performance with L1 signals could hardly meet the requirement that whole risky groups would be detected by confirming the contour analyses in Figure 6(a) and Figure 6(b). Similar results for dual-station smoothing with the 100-second metric-smoothing process and lower F_S value of 48 MHz are shown in Figure 12(b), indicating that a combination of

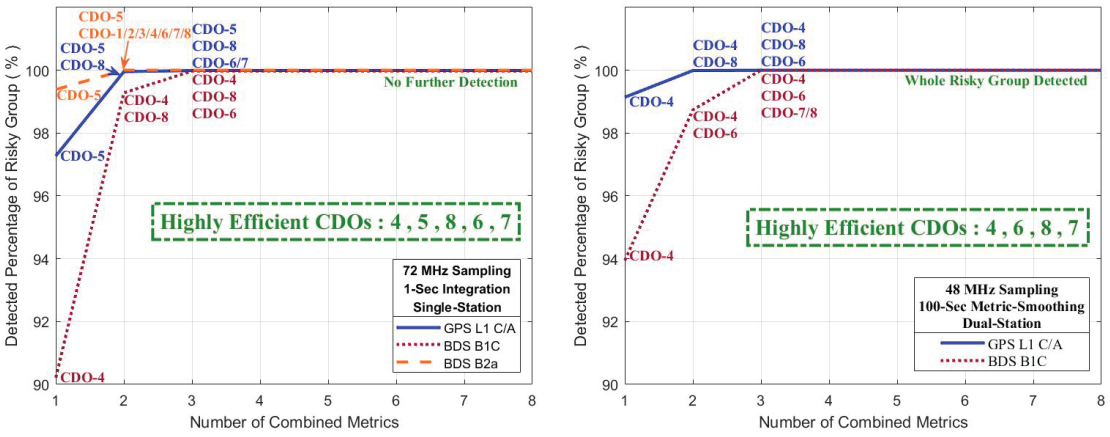

(a) Critical Detection Ability

(b) Combined Detection Ability

FIGURE 12 Examinations on the detection ability of CDOs

TABLE 9
Generic CDO-Based SQM Algorithms for Dual-Frequency Civilian Signals

ITEMS			CONFIGURATIONS		
Name			SCSQM8r		
Carrier frequency			L1/B1		L5/B2
Correlator	**Observable**		CDO		
	Location (chips)	**Baseline**	±1/80, ±3/80, ±5/80, ±7/80		±1/8, ±3/8, ±5/8, ±7/8
		Simplified	−1/80, +1/80, +3/80, +5/80, +7/80		−1/8, +1/8, +3/8, +5/8, +7/8
Integration period (seconds)			1		
Detection metrics		**Baseline**	8		
		Simplified	5		
Metric-smoothing	**Period** (seconds)		100		—
	Improvement factor		1.5 – 2.3		
Signal			GPS L1 C/A	BDS B1C MEO	BDS B2a MEO
Theoretical minimum receiving C/N_0 (dB-Hz)			39	37.5	39.3
Sampling frequency (MHz)			≥33		
Reference-smoothing stations		**SIF = 1.5**	$\lceil (0.0199 \cdot F_S + 0.0176)^{-2} \rceil$	$\lceil (0.0151 \cdot F_S + 0.0055)^{-2} \rceil$	—
		SIF = 2.3	$\lceil (0.0306 \cdot F_S + 0.0270)^{-2} \rceil$	$\lceil (0.0231 \cdot F_S + 0.0084)^{-2} \rceil$	
Probability of false-alert			1.5×10^{-7} per test		
Probability of miss-detection			1×10^{-3} per test		
MERR (meters)			1.61		2.89

three CDOs (i.e., CDO-4, CDO-6, and CDO-8) are enough to protect the integrity of L1 signals as long as all the conditions are set in correspondence with the designed baseline algorithm.

A group of simplification attempts were carried out as indicated by the design flow in the upper part of Figure 3, of which two examples were briefly introduced. The most efficient were CDO-4 and CDO-5, followed by CDO-8 and CDO-6, and the less efficient CDO-7 as well. Given these tests on CDO-sensitivity, the baseline algorithm can be simplified to a version with only five metrics/CDOs. Both the CDO-based SQM algorithms for dual-frequency civilian signals are summarized in Table 9. The formula for the term "SIF = 1.5" of reference-smoothing stations are based on the linear fitting in Figure 9. Those with the term "SIF = 2.3" are similar.

6 | CONCLUSION AND FUTURE WORK

Aiming at mitigating signal deformation risks for safety-critical users under DFMC SBAS criteria, we proposed a design methodology for CDO-based SQM methods on the basis of derivation, simulation, and simplification. A complete and general algorithm was designed in accordance with the proposed methodology and its performance was confirmed under the specified TMs and TSs of three differently modulated representative civilian signals with the given receiver configuration space.

The proposed design methodology was guided by the a-priori procedure of operational CDO-based SQM. After the separation and classifying processes, the

influential factors needed for design were clarified, and then the route of design was determined. Core sections of the proposed design methodology were the determination of the generally optimal code-phase bin length and the smoothing processes. The former determination was achieved through massive simulations carried out by a specially designed verification platform. For the smoothing processes, reference-smoothing conditions were found to be sampling dependent, given a fixed conservative improvement of metric-smoothing.

The performance estimates of the designed algorithm were obtained from simulations and also compared to those of the traditional method. Based on the verified correctness and effectiveness of the designed baseline algorithm by a group of assessments, a demonstration of simplification processes was executed to find the most efficient metrics/CDOs and/or combinations to reduce implementation complexity.

The proposed design methodology of CDO-based SQM method provides a normal form for particular signals toward given requirements. Some aspects of envisioned future work are listed as follows:

- exploiting the potential of CDO-based SQM using more complicated detection metrics or varying the number of CDOs to result in various optimal sectionalizing schemes
- utilizing live data from multiple featured multipath environments to investigate time-varying smoothing improvements
- applying the proposed design methodology to other civilian signals such as GPS L5-Q, GLONASS L1OCd and L3OC, and Galileo E1-C and E5a-Q

ACKNOWLEDGMENTS

This work was supported by the National Key R&D Program of China under Grant No. 2021YFA0716603. The authors would like to thank all the editors and reviewers for their patience, professionalism, and constructive comments. We also want to thank Dr. Sihao Zhao, a research associate with the Department of Electrical, Computer, and Biomedical Engineering at Ryerson University, for his sincere and beneficial help in the revision of this article.

REFERENCES

Cui X. W. (2020). *Applicability analysis of the filter gain roll-off in DFMC SBAS receiver design constraints for BDS B1C and B2a signal* [Working paper]. ICAO.

Fenton, P. C., & Jones, J. (2005). The theory and performance of NovAtel Inc.'s Vision Correlator. *Proc. of the 18th International Technical Meeting of the Satellite Division of the Institute of Navigation (ION GNSS 2005)*, Long Beach, CA, 2178–2186. https://www.ion.org/publications/abstract.cfm?articleID=6420

Fontanella, D., Paonni, M., & Eissfeller B. (2010). A novel evil waveforms threat model for new generation GNSS signals: theoretical analysis and performance. *2010 5th ESA Workshop on Satellite Navigation Technologies and European Workshop on GNSS Signals and Signal Processing (NAVITECH),* Noordwijk, Netherlands. https://doi.org/10.1109/NAVITEC.2010.5708037

He, C. Y., Guo, J., Lu, X., Wang, X., Rao, Y., Kang, L., & Hu, Z. (2018). A new evil waveforms evaluating method for new BDS navigation signals. *GPS Solutions*, 22. https://doi.org/10.1007/s10291-018-0698-x

International Civil Aviation Organization (ICAO). (2006). *International standards and recommended practices: Annex 10 to the convention on international civil aviation – aeronautical telecommunications* (6th Ed., Vol. 1). ICAO.

International Civil Aviation Organization (ICAO). (2018). *DFMC SBAS SARPs – part B* (Working Paper No. DS2/WP/3 v2.0). DFMC SBAS SARPs Sub Group (DS2). ICAO. https://www.icao.int/airnavigation/Documents/NSP5_Report%20on%20Agenda%20Item%202.APPENDIX%20A2%20-%20DFMC%20SBAS%20SARPS%20Part%20B.pdf

Li, R., Tang, X., & Ou, G. (2017). GNSS signal quality analysis technique based on chip measurement. *2017 IEEE 3rd Information Technology and Mechatronics Engineering Conference (ITOEC)*, Chongqing, China. https://doi.org/10.1109/ITOEC.2017.8122339

Pagot, J. -B., Thevenon, P., Julien, O., Gregoire, Y., Fernández, F. A., & Maillard, D. (2015). Estimation of GNSS signals' nominal distortions from correlation and chip domain. *Proc. of the 2015 International Technical Meeting of the Institute of Navigation,* Dana Point, CA, 415–427. https://www.ion.org/publications/abstract.cfm?articleID=12640

Pagot, J. -B., Thevenon, P., Julien, O., Amarillo-Fernández, F., & Maillard, D. (2016). Threat models design for new GNSS signals. *Proc. of the 2016 International Technical Meeting of the Institute of Navigation,* Monterey, CA, 970–982. https://doi.org/10.33012/2016.13476

Pagot, J. -B. (2016). *Modeling and monitoring of new GNSS signal distortions in the context of civil aviation* [Doctoral dissertation, University of Toulouse]. HAL theses. https://tel.archives-ouvertes.fr/tel-01528481

Pagot, J. -B., Julien, O., Thevenon, P., Fernandez, F. A., & Cabantous, M. (2018). Signal quality monitoring for new GNSS signals. *NAVIGATION*, *65*(1), 83–97. https://doi.org/10.1002/navi.218

Phelts, R. E. (2001). *Multi-correlator techniques for robust mitigation of threats to GPS signal quality* [Doctoral dissertation, Stanford University]. Stanford University Archives. https://web.stanford.edu/group/scpnt/gpslab/pubs/theses/EricPheltsThesis01.pdf

Phelts, R. E., Walter, T., & Enge, P. (2003). Toward real-time SQM for WAAS: improved detection techniques. *Proc. of the 16th International Technical Meeting of the Satellite Division of the Institute of Navigation (ION GPS/GNSS 2003)*, Portland, OR, 2739–2749. https://www.ion.org/publications/abstract.cfm?articleID=5462

Phelts, R. E., Wong, G., Walter, T., & Enge, P. (2013). Signal deformation monitoring for dual-frequency WAAS. *Proc. of the 2013 International Technical Meeting of the Institute of Navigation*, San Diego, CA, 93–106. https://www.ion.org/publications/abstract.cfm?articleID=10817

Selmi, I., Thevenon, P., Macabiau, C., Julien, O., & Mabilleau, M. (2020). Signal quality monitoring algorithm applied to Galileo signals for large evil waveform threat space. *Proc. of the 2020 International Technical Meeting of the Institute of Navigation*, San Diego, CA, 352–365. https://doi.org/10.33012/2020.17149

Shallberg, K. W., Ericson, S. D., Phelts, E., Walter, T., Kovach, K., & Altshuler, E. (2017). Catalog and description of GPS and WAAS L1 C/A signal deformation events. *Proc. of the 2017 International Technical Meeting of the Institute of Navigation*, Monterey, CA, 508–520. https://doi.org/10.33012/2017.14877

Sun, C., Zhao, H., Feng, W., & Zhuang, C. (2016). A novel digital threat model and effect analysis on modernized BeiDou signals. *Proc. of the 2016 International Technical Meeting of the Institute of Navigation*, Monterey, CA, 401–413. https://doi.org/10.33012/2016.13426

Thevenon, P., Pagot, J. -B., Julien, O., & Tessier, Q. (2014). Processing technique and performance of the observation of evil waveform in the chip domain. *Proc. of the 7th ESA Workshop on Satellite Navigation Technologies*, Noordwijk, Netherlands. https://hal-enac.archives-ouvertes.fr/hal-01094193

Walter, T., Blanch, J., Phelts, R. E., & Enge, P. (2012). Evolving WAAS to serve L1/L5 users. *NAVIGATION,* 59(4), 317–327. https://doi.org/10.1002/navi.21

Wang, X., Gao, Y., Cui, X., Liu, G., & Lu, M. (2021a). A signal quality monitoring algorithm based on chip domain observables for BDS B1C signal. *Proc. of the 2021 International Technical Meeting of the Institute of Navigation*, Virtual, 149–161. https://doi.org/10.33012/2021.17810

Wang, X., Cui, X., Wei, K., Liu, G., Gao, Y., & Lu, M. (2021b). Signal quality monitoring algorithms of DFMC SBAS for dual-frequency civil signals of BDS. In C. Yang & J. Xie (Eds.), *China Satellite Navigation Conference (CSNC 2021) Proceedings: Volume II.* Lecture Notes in Electrical Engineering (Vol. 773, pp. 75–91). Springer. https://doi.org/10.1007/978-981-16-3142-9_8

Wei, K., Cui, X., Wen, J., & Lu, M. (2020). A research on modeling and monitoring of new BDS B1C signal distortions in the context of BeiDou satellite based augmentation system. *Proc. of the 2020 International Technical Meeting of the Institute of Navigation,* San Diego, CA, 341–351. https://doi.org/10.33012/2020.17148

Weill, L. R. (2007). Theory and applications of signal compression in GNSS receivers. *Proc. of the 20th International Technical Meeting of the Satellite Division of the Institute of Navigation (ION GNSS 2007),* Fort Worth, TX, 708–719. https://www.ion.org/publications/abstract.cfm?articleID=7571

Xie, G. (2004). *Optimal on-airport monitoring of the integrity of GPS-based landing systems* [Doctoral dissertation, Stanford University]. Stanford University Archives. https://web.stanford.edu/group/scpnt/gpslab/pubs/theses/GangXieThesis04.pdf

How to cite this article: Wang, X., Cui, X., Liu, G., Wei, K., & Lu, M. (2022). Signal quality monitoring based on chip domain observables: theory, design, and implementation. *NAVIGATION, 69*(4). https://doi.org/10.33012/navi.543

APPENDIX A | DERIVATION OF THE APPROXIMATE MEAN OF THE EIGHT MDES

The sample points of the RF front-end output were considered to be affected by additive white Gaussian noise (AWGN). On nominal code signals, the standard deviation of the AWGN is given by:

$$\sigma_{\text{AWGN}}^2 = \frac{1^2}{SNR} = \frac{1}{10^{\frac{C/N_0}{10}} \Big/ \left(BW/2\right)} = \frac{BW}{2} \cdot 10^{-\frac{C/N_0}{10}} \tag{A1}$$

where SNR is the signal-to-noise ratio, C/N_0 is the considered carrier-to-noise ratio, and BW is the double-sided pre-correlation bandwidth. A sixth-order Butterworth filter was applied as the pre-correlation filter. Then, the power of noise was expressed as:

$$\sigma_{\text{filtered}}^2 = \sigma_{\text{AWGN}}^2 \cdot \frac{BW}{F_S} = \frac{BW^2}{2 \cdot F_S} \cdot 10^{-\frac{C/N_0}{10}} \tag{A2}$$

where F_S is the sampling frequency of the RF front-end output. Considering the CDO measurement and normalization processes expressed by Equation (3) and Equation (4) in the main text, the standard deviation of a raw CDO is given by:

$$\sigma_{\text{CDO}_i} = \frac{\sigma_{\text{filtered}}}{I_p \cdot \sqrt{N_{\text{bin}_i}^{\text{samp}}}} = \frac{BW}{I_p \cdot \sqrt{2 \cdot F_S \cdot N_{\text{bin}_i}^{\text{samp}}}} \cdot 10^{-\frac{C/N_0}{20}} \tag{A3}$$

where $1 \le i \le M$ represents one of the M code-phase bins of a chip and $N_{\text{bin}_i}^{\text{samp}}$ is the number of digitized sample points collected by bin_i within the specified integration period, T_{int}.

The total amount of sample points with one period of integration is expressed by:

$$N_{\text{total}}^{\text{samp}} = F_S \cdot T_{\text{int}} \tag{A4}$$

Since we only apply the CDOs on rising edge, the concept of rising edge rate (RER) was introduced. By focusing on the section from -0.5 to +0.5 chips around a rising edge, the considered number of sample points in all the bins is given as:

$$\sum_{i=1}^{M} N_{\text{bin}_i}^{\text{samp}} = F_S \cdot T_{\text{int}} \cdot \text{RER} \tag{A5}$$

Define BIN to be the proportion of a bin length to a chip. The average number of sample points participating in calculating a CDO is given by:

$$\bar{N}_{\text{CDO}}^{\text{samp}} = F_S \cdot T_{\text{int}} \cdot \text{RER} \cdot \text{BIN} \tag{A6}$$

With accordance to Equation (8) in the main text, the approximate mean of the eight MDEs can be given as:

$$\begin{aligned} \overline{\text{MDE}} &= \left(K_{\text{ffd}} + K_{\text{md}}\right) \cdot \bar{\sigma}_{\text{CDO}} \\ &\approx \frac{\left(K_{\text{ffd}} + K_{\text{md}}\right) \cdot BW}{I_P \cdot F_S \cdot \sqrt{2 \cdot T_{\text{int}} \cdot \text{RER} \cdot \text{BIN}}} \cdot 10^{-\frac{C/N_0}{20}} \end{aligned} \tag{A7}$$

where K_{ffd} and K_{md} are the quantiles of the required probabilities of fault-free detection and miss-detection. This means that the MDE is applied for critical performance investigation.

APPENDIX B | DEFINITIONS OF THE FEATURED LENGTHS FOR CONSTRAINTS ON SELECTION OF CODE-PHASE BIN LENGTH WITH NOMINAL SIGNALS

In order to give constraints on the selection of code-phase bin length with nominal signals, two featured lengths (i.e., Δ_1^{nom} and Δ_2^{nom} in time domain) are defined from simulations, standing for the two segments with the most rapid change on a rising edge, as shown in Figure B1.

First, an ideal rectangular GPS L1 C/A code waveform is filtered by a sixth-order Butterworth filter and a cross-correlating process is performed, from which a delay of about 0.0526 chips introduced by the filter is measured. By mapping this delay to the filtered chip waveform, the prompt point in the time domain was obtained, corresponding to the prompt correlator.

Then, the two featured lengths were measured. Δ_1^{nom} is the length between the prompt point and the overshoot point after filtering and Δ_2^{nom} is the length between the overshoot point and the highest point after one period of damped oscillation. The lengths of about 0.0429 chips and 0.0885 chips were measured from the filtered chip waveform, respectively. Since these two featured lengths together stand for the segment with the fastest change on a rising edge, it can be considered that the oscillation information contained by these two segments would be the main part.

To determine the weight of this main part, we introduced the third featured length, Δ_3^{nom}, as shown in Figure B1. Conventionally, we think a damped oscillation

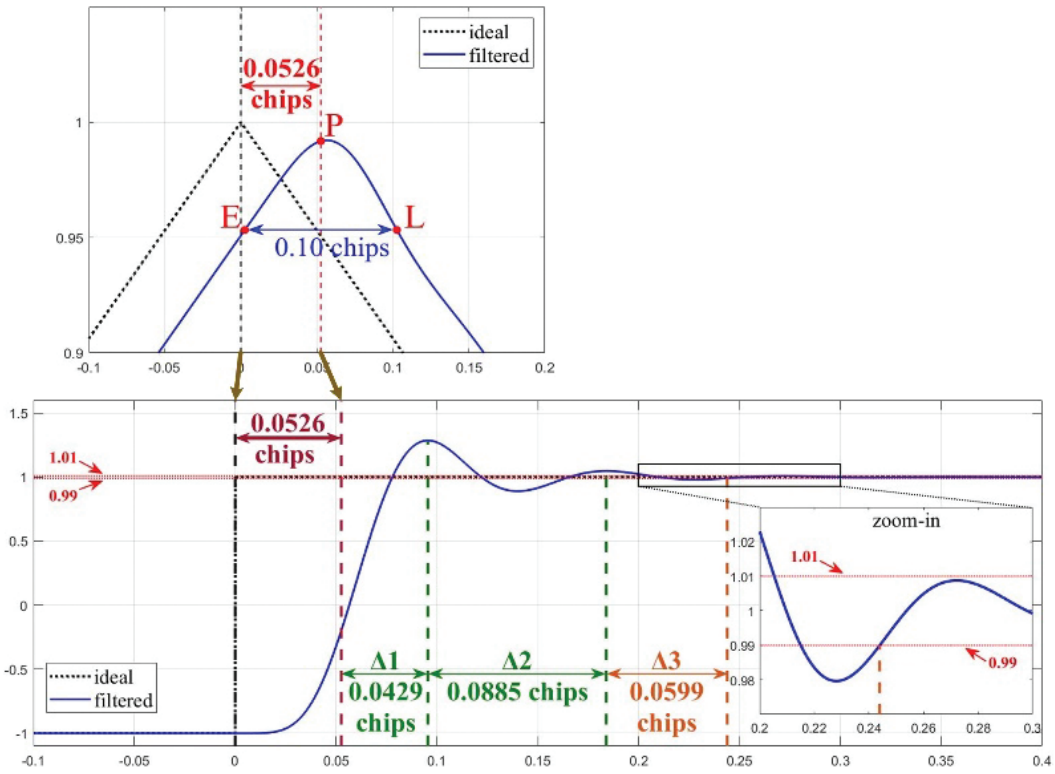

FIGURE B1 Illustration of the featured lengths with nominal signal

has converged when the magnitudes do not exceed ±1% of the steady value. Then, Δ_3^{nom} is measured to be 0.0599 chips. Since:

$$\frac{\Delta_1^{\text{nom}} + \Delta_2^{\text{nom}}}{\Delta_1^{\text{nom}} + \Delta_2^{\text{nom}} + \Delta_3^{\text{nom}}} \approx 68.69\% \tag{A8}$$

this value is near the 1σ percentage of 68.27% that was determined to be used as the weight.

APPENDIX C | RESULTS OF ASSESSMENTS FOR L1 SIGNALS

TABLE A1
Assessment Results of L1 Signals

Sgn	F_S	Ref-Smt		Mtr-Smt Gain (dB)	Theo_Min_C / N_0		Min_Eqv_C / N_0	Asmt Result
		N_{ref}	Gain (dB)		Rcv	SQM	(dB-Hz)	
GPS L1 C/A	72	1	0.0	4.0	39.0	43.0	39.5	bound
	69	1	0.0				40.0	bound
	66	1	0.0				39.8	bound
	63	1	0.0				40.2	bound
	60	1	0.0				40.8	bound
	57	1	0.0				41.5	bound
	54	1	0.0				41.9	bound
	51	1	0.0				42.2	bound
	48	2	3.0			46.0	43.1	bound
	45	2	3.0				43.4	bound
	42	2	3.0				43.8	bound
	39	2	3.0				44.1	bound
	36	2	3.0				45.3	bound
	33	3	4.8			47.8	46.2	bound
BDS B1C	72	1	0.0	4.0	37.5	41.5	40.3	bound
	69	1	0.0				40.6	bound
	66	1	0.0				41.1	bound
	63	2	3.0			44.5	41.6	bound
	60	2	3.0				41.9	bound
	57	2	3.0				42.4	bound
	54	2	3.0				42.8	bound
	51	2	3.0				43.3	bound
	48	2	3.0				43.8	bound
	45	3	4.8			46.3	44.6	bound
	42	3	4.8				45.0	bound
	39	3	4.8				45.6	bound
	36	4	6.0			47.5	46.4	bound
	33	4	6.0				46.8	bound

Note: The terms *Ref-Smt* and *Mtr-Smt* refer to the reference-smoothing and metric-smoothing processes, respectively. The theoretical minimum C/N_0 for either ground receivers or SQM-detection equivalency is included in the term Theo_Min_C/N_0.